Design of Optical Measurements for Plasma Actuators for the Validation of Quiescent and Flow Control Simulations

Derrick C. Lam

Thesis submitted to the Faculty of the

Virginia Polytechnic Institute and State University

in partial fulfillment of the requirements for the degree of

Master of Science

in

Nuclear Engineering

Leigh Winfrey, Chair

Mark Pierson

Yang Liu

December 09, 2015

Blacksburg, Virginia

Keywords: Plasma diagnostics, spectroscopy, spectrometer, electron temperature, electron density, 3D printed, experimental, simulation, quiescent, flow control, plasma actuator, OES, optical emission spectroscopy.

Design of Optical Measurements for Plasma Actuators for the Validation of Quiescent and Flow Control Simulations

Derrick C. Lam

(ABSTRACT)

The concept of plasma flow control is a relatively new idea based on using atmospheric plasma placed near the edge of an air foil to reduce boundary layer losses. As with any new concept, it is important to be able to quantify theoretical assumptions with known experimental results for validation. Currently there are a variety of experiments being done to better understand plasma flow control, but one particular experiment is through the use of multi-physics modeling of dielectric barrier discharge actuators. The research in this thesis uses optical measurement techniques to validate computational models of flow control actuators being done concurrently at Virginia Tech.

The primary focus of this work is to design, build and test plasma actuators in order to determine the plasma characteristics relating to electron temperatures and densities. Using optical measurement techniques such as plasma spectroscopy, measured electron temperatures and densities to compare with theoretical calculations of plasma flow control under a variety of flow conditions. This thesis covers a background of plasma physics, optical measurement techniques, and the designing of the plasma actuator setups used in measuring atmospheric plasmas.

Dedication

I would like to dedicate my thesis work to my family and friends. I especially like express my gratitude to my parents, Samona and Alan Lam who have always encouraged and had faith in me to never stop learning and to always better myself as a person. I look forward to when I have the chance to show them the work I have been able to do thanks to their love and care throughout my life. I would also like to express my gratitude to Antarjot for her support and encouragement in my endeavors and for always brightening my day.

Acknowledgments

Contents

5 Bibliography 51

List of Figures

List of Tables

Chapter 1

Introduction

1.1 Project Introduction

Optical emission spectroscopy (OES) is an *in situ* non-invasive diagnostic technique that uses atomic emissions to determine the elemental composition of a sample. In this thesis, the sample being studied is atmospheric plasma produced using a pulsed Direct Current (DC) Dielectric Barrier Discharge (DBD) actuator. The atmospheric plasma created, using a DBD actuator, has a wide variety of applications in flow control within gas turbines, struts, airfoils, inlets, and a variety of low Reynolds number flow applications [1-3, 8, 13]. Although the research in this paper is with flow control using a DBD actuator in mind, atmospheric plasmas have additional interests that include but are not limited to the bio-medical and environmental industry for controlling air pollution, waste water cleaning, bio-

decontamination, material/surface treatment, electromagnetic wave shielding, and nanotube growth [4-7]. Since the current use of DBD actuators as a form of plasma generation for flow control is still a relatively novel technique, this study will focus on the ability to quantify the generated plasma, using OES to allow for the validation and comparison of important plasma parameters in on-going and concurrent research of multi-physics modeling of DBD flow control actuators. [46]

In order to gather data for use in quantifying the plasma generated, two optical measurement methods were used, OES and shadowgraphy. OES was used due to its ability to receive data in an in situ and non-invasive manner as to not obstruct air and plasma flow and affect the boundary layers surrounding the actuator. Additionally, the use of shadowgraphy using a high speed camera was used to look at and analyze the characteristic flow produced by the generating plasma for determining velocities and comparing the vortex structure with those produced in simulated multi-physics models. However, the main focus of this thesis will be in using OES for the determination of plasma parameters.

For this experimental research, a DBD actuator, a quiescent actuator holder, and flow tunnel setup were designed and built. Figure 1.1 shows the quiescent on the left and flow tunnel on the right and the associated optical measurement equipment. The quiescent actuator setup consisted of a 3D printed holder for the actuator that stabilized all of the degrees of freedom of the actuator except for movement in the horizontal one dimensional position for assembly and aligning with the spectrometer fiber-optic cable, which was stabilized and held at the intersection of the four arches. In order to reduce background interference from outside light
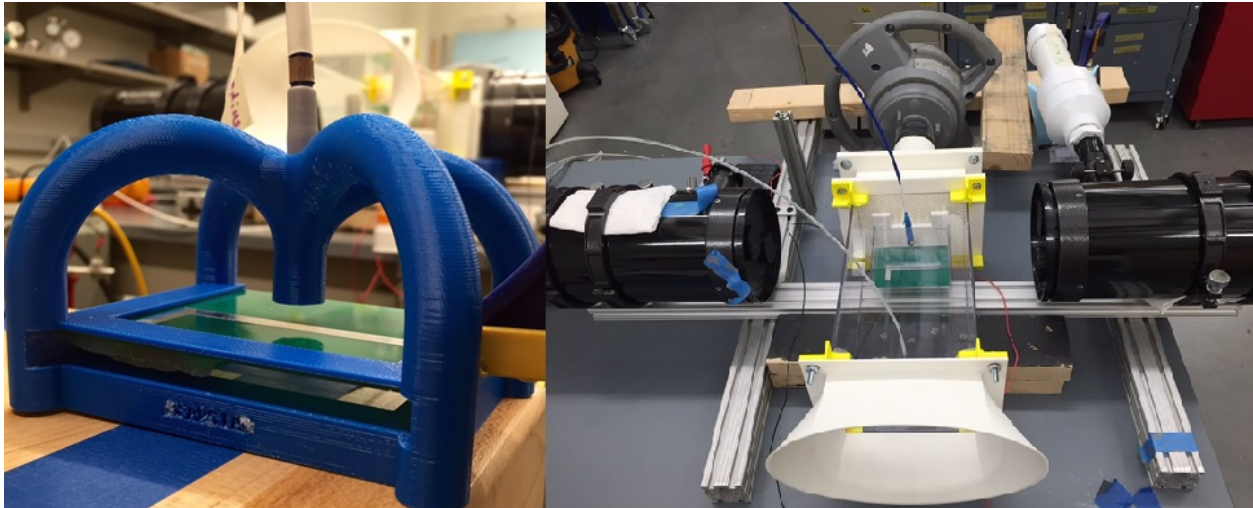
Figure 1.1: A picture of the quiescent plasma actuator setup with spectrometer fiber-optic holder on the left and the flow tunnel setup with the shadowgraphy setup and spectrometer holder on the right.

sources and to ensure no moving air, the entire setup was covered by a hand built dark chamber. In addition to the 3D printed holder for spectroscopy use, a completely sealed acrylic test box was built for testing in a quiescent condition for use with the shadowgraphy setup.

The flow tunnel setup consisted of six separate parts as seen in Figure 1.2. From left to right, the first piece is a 3D printed bell mouth inlet for smoothing inlet air to maintain laminar inlet wall boundaries. The second piece is a hand built clear acrylic tunnel that allowed the use of shadowgraphy. The third piece is a 3D printed honeycomb setup that suspended the actuator setup and helped stabilize turbulent air produced by the shop vacuum. The fourth piece is the plasma actuator setup consisting of clear acrylic attached to the actuator and bolted to the front of the honeycomb and covered by the second piece of acrylic tunnel. The
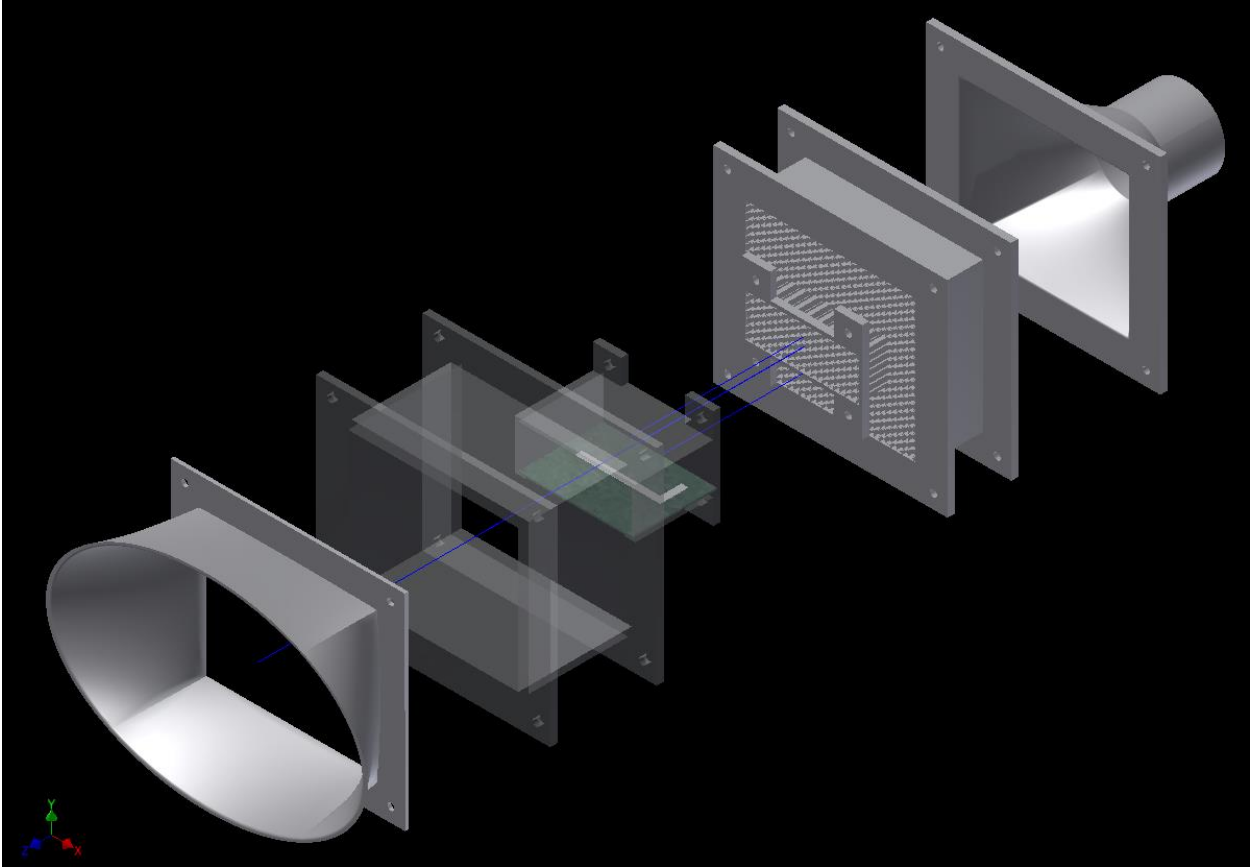
Figure 1.2: A exploded view of the flow tunnel setup minus the shop vacuum. From left to right the pieces are: the bell mouth inlet, acrylic shadowgraphy tunnel, plasma actuator assembly, honeycomb, and rectangular to circular adapter.

fifth piece is a rectangular to circle adapter for use in connecting the entire tunnel assembly to the shop vacuum. The sixth piece is the shop vacuum which provides the vacuum to generate the flow of air across the actuator. The data gathered from this experimental research allows for the quantification of plasma parameters for comparison and validation of multi-physics model simulations of DBD actuators.

1.2   Plasma Background

The word plasma comes from the Greek word that means "that which is molded" and plasmas in physics are considered to be the fourth state of matter. In physics, the state of materials when there is very little to no energy applied to them has the form of a solid material such as ice. As energy is applied to that material, its molecules will go from a near stationary state in absolute zero or freezing temperatures to a liquid state such as water in room temperature. If additional energy is applied to the material, then the state will change from liquid to a gas such as water to its gaseous state in the form of steam. If more energy is applied, then the fourth state of matter will be achieved, where the molecules and atoms will go through a process of ionization, which is when electrons are added or removed. A basic molecular representation of the states of matter can be seen in Figure 1.3.

If electrons are added to an atom, it is considered to be in an excited state, and excited states can be met through various conditions such as atomic collisions, electrical currents, and high
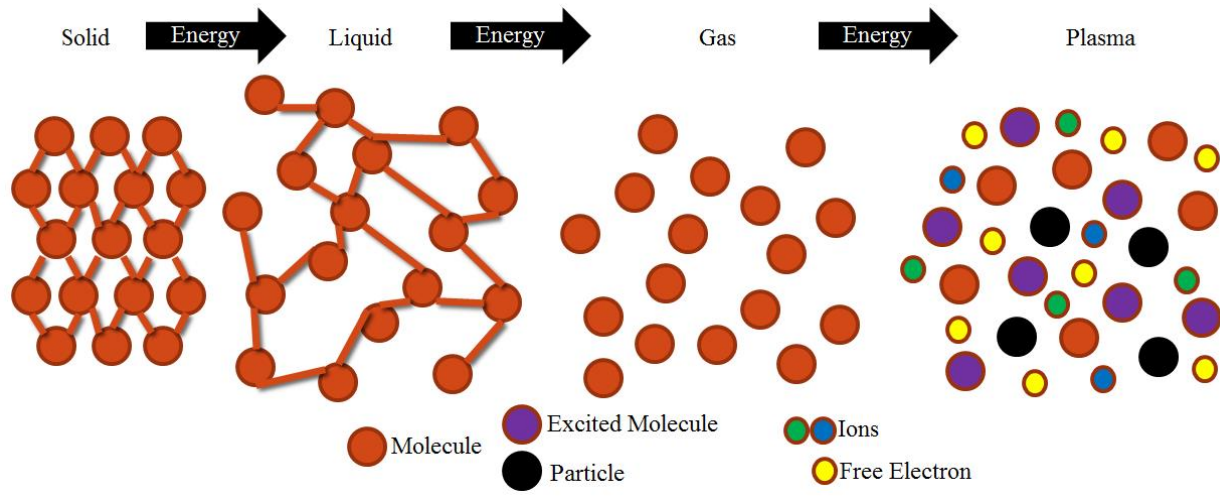
Figure 1.3: A basic molecular representation of molecule transition states as energy is applied to each system where the fourth state of matter is plasma.

temperatures. As molecules and atoms gain electrons and become charged particles, they will tend to move in specific concentrations of positive or negatively charged groups. As these charged particles tend to separate into the two groups they will produce their own electric fields which also lead to their own magnetic field being produced. As a result of the magnetic fields and currents, the charged particles will exhibit a collective behavior that allows them to be molded in the presence of other magnetic fields. [9-11, 24, 30, 32-34, 36]

1.3   Plasma Actuators

Typically in flow control, a plasma actuator takes the form of circuit board with an exposed electrode layer that ionizes the air particles within the region around the electrode. As a

source of power, actuators can use Alternating Current (AC) or DC power sources and the power can be delivered over time as a series of rapid pulses or as non-pulsed steady state source. Once the air particles are ionized into a plasma, the plasma generated along the length of the electrode will move with a local spinning in the form of a vortex along the surface of the circuit board away from the electrode source at some velocity. [12, 13]
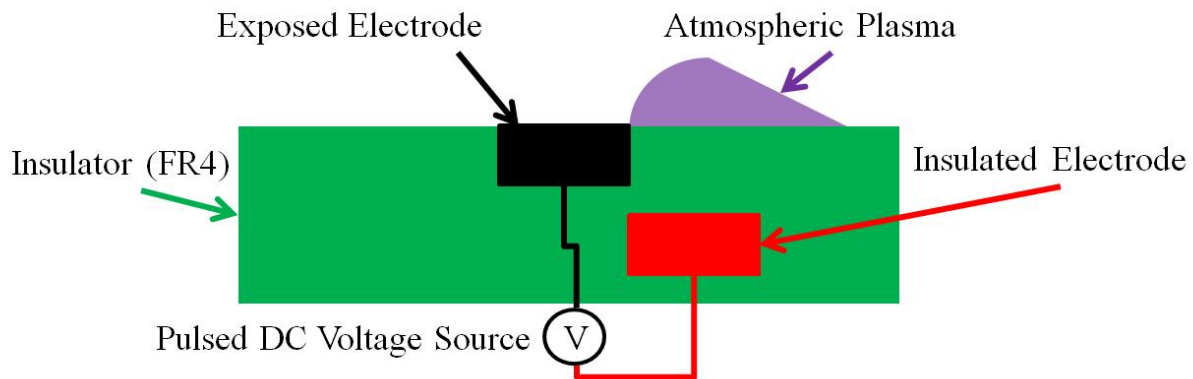
Figure 1.4: Schematic of a basic DBD plasma actuator where the insulator is a typical epoxy circuit board layer (FR4) that acts as the dielectric barrier encompassing the ground and input electrode. As power is sent via a pulsed DC voltage source through the red electrode within the circuit board and grounded via the black electrode, the exposed side of the black electrode ionizes the air within its vicinity to generate an atmospheric that moves from left to right in this case.

As a result, the plasma generated from the electrode is able to help reduce any potential boundary layer losses if placed in a situation where there is some type of air flow around the vicinity of the actuator. An example shown in Figure 1.4 is a schematic of a basic plasma actuator orientation with plasma flow moving from left to right as air is ionized into a plasma

around the grounded exposed electrode. The plasma bubble will be generated at the leading edge of the exposed electrode and over the insulated electrode area.

1.4   Optical Emission Spectroscopy

Using OES, a spectrometer is able to receive photons from de-exciting atoms given off from the plasma. Each of the photons given off by de-exciting atoms has a unique wavelength and unique energy that is special to the element of its origin. Figure 1.5 shows a visualization of the excitation of an atom from its base state of E1 to an excited state of E2 through some change in energy. As the excited state de-excites from state E2 to E3, it gives off its excess energy in the form of a photon hv, where a photons energy is defined as Plancks constant h times the frequency v. [14, 15, 29, 31]

The photons are received and transmitted to the spectrometer via a fiber-optic sensor cable. Once the data is received by the spectrometer, the photons are organized as a series of intensity values at specific wavelengths and energies. Using software associated with the spectrometer and databases, such as the National Institute of Standards and Technology (NIST), the intensity value, energy, and wavelength of photons can be associated with specific atomic elements and their ionization levels such as neutral oxygen, singly ionized nitrogen, and ect. Once data is received and analyzed using the spectrometer, the data can be used to calculate the plasma temperature and plasma densities. [16, 24-27, 35,37]
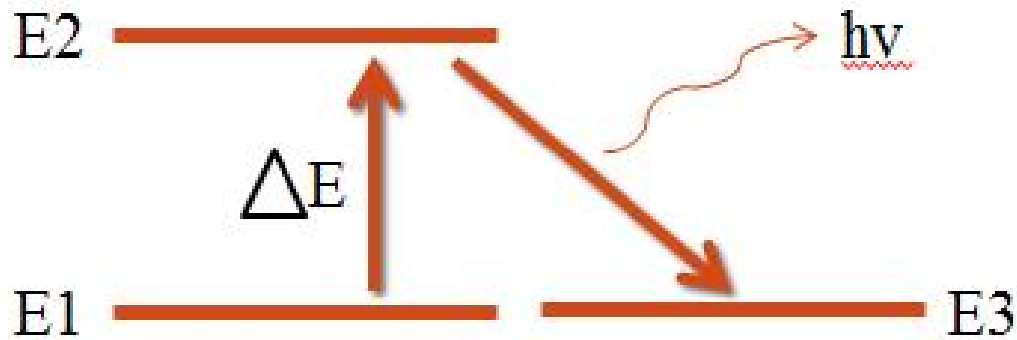
Figure 1.5: Visual representation of the levels of excitation experienced by an atom when receiving an addition electron to become excited (E1 to E2), and the resulting photon hv produced as it de-excites (E2 to E3) back to its original state.

1.5 Shadowgraphy

Shadowgraphy is an optical imaging technique where the use of a light source is projected on to an object such that the shadow created can be observed and recorded. Typically, a shadowgraph setup consists of a bright light source, multiple pieces of optics in the form of glass or mirrors to focus the projected light, and a method to view and record the shadow produced. When light is focused and projected onto an object, a shadow is produced, but in the case of analyzing an opaque medium such as a plasma or even air, the light passing through the medium will be slowed down and refracted differently depending on its density. This difference results in a difference in the speed of the light when it reaches the end. Upon

reaching the end where a viewing device is located, the differences in density can be observed. A schematic of the shadowgraph system can be seen in Figure 1.6 An example similar to shadowgraphy is when a person looks down a black tarmac road on a very hot day. What can be seen are the changes in air density as light gets refracted by less dense air molecules rising from the tarmac. [17, 18] The additional use of a high speed camera to record the changes in density of the medium observed can be used to determine velocities if the size of the viewing area and change in time is known.

1.6   Project Scope

As mentioned earlier, the primary focus of this thesis is to use optical measurement techniques, such as OES, in the determination of the plasma parameters in the experimental DBD actuator setup. Calculated plasma parameters, such as temperature and density, based on experimental data can be compared to the plasma temperature and plasma density produced by multi-physics model simulations that are being performed concurrently at Virginia Tech (VT) to validate theoretical calculations are operating under proper assumptions and producing accurate results. Additionally, the scope of this project is to be able to apply known measurement techniques to consistently calculate accurate plasma parameters for a relatively new platform that has little measured data as of today without the use of a seed gas or introducing a lot of energy into the system.
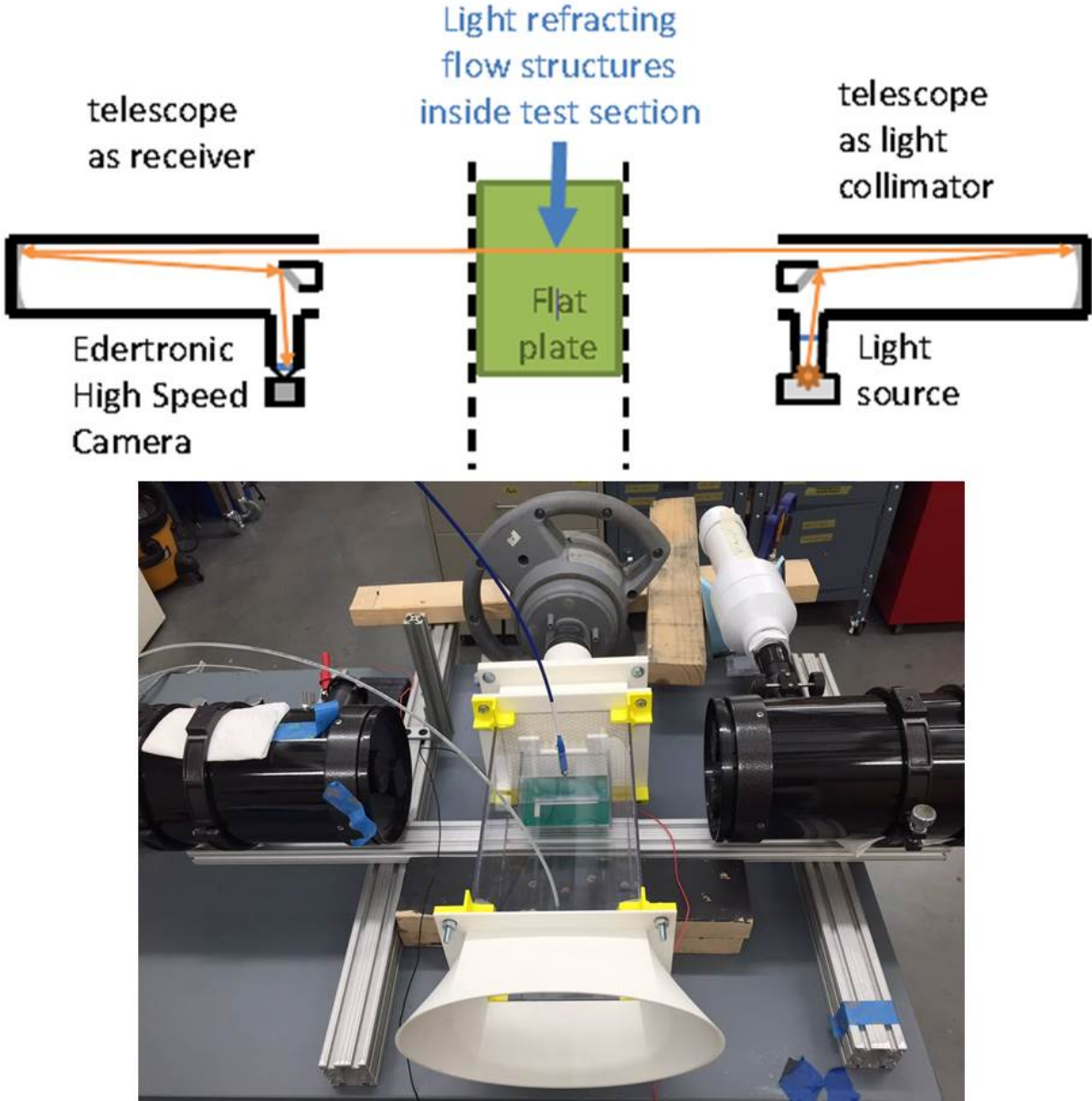
Figure 1.6: Schematic of the shadowgraphy system compared with the physical shadowgraphy setup.

Chapter 2

Experimental Methods

2.1 Equipment Specifications

The optical emission equipment consists of a Ocean Optics LIBS2500Plus Laser-induced Breakdown Spectrometer, which has a spectral range of $200 - 980nm$, with a resolution of approximately $0.1nm$ at full width half maximum (FWHM) and a sensitivity of parts-per-billion (ppb) and picogram levels. [19] Figure 2.1 Shows the LIBS2500 Plus used in taking spectral data. Even though the name of the spectrometer is labeled as laser-inducing and spectrometer is capable of being used in conjunction with a high powered pulsed laser to ablate a material to create a plasma for plasma diagnostic purposes, in this research the laser producing the plasma is replaced by the pulsed DC DBD actuator. The spectrometer consists of seven spectrometer channels. The spectral range capability of the spectrometer,

$200 - 980nm$, is divided into seven regions. Each channel has its own fiber-optic cable lead where all seven converge into one for sensing emitted photons. The OceanView software is used to manage and record the data outputted by the LIBS2500Plus Spectrometer, and Mikropack Specline is used to analyze the raw spectral data to determine the individual constituents in the generated plasma.
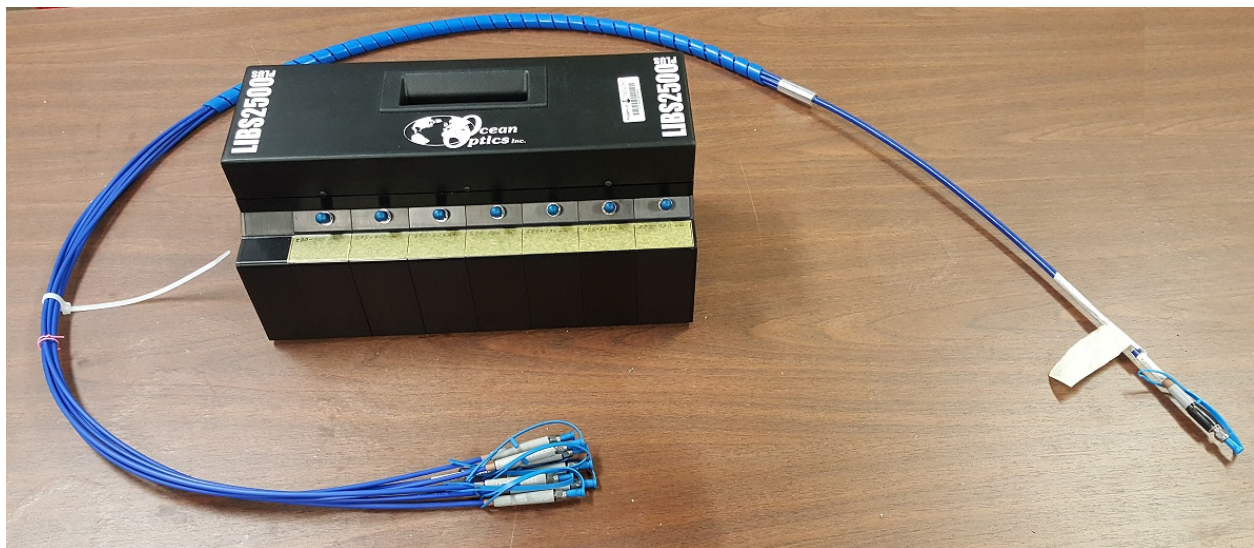
Figure 2.1: Photo of the OceanOptics LIBS2500 Plus spectrometer and fiber-optic cable.

Additionally a B&K Precision 4030 10Mhz Pulse Generator, Tektronix TPS2024B Oscilloscope, Dell 135w PSU, Tektronix P6015A High Voltage Probe were used to regulate power input, monitor current, deliver the power, and measure the voltage respectively. The plasma actuator setup consists of a custom printed two layer printed circuit board. To hold, stabilize and align the spectrometer sensor with the actuator, a cradle for the actuator and spectrometer fiber optic cable was designed and printed in ABS plastic using additive manufacturing from a Stratasys Dimension uPrint 3D Printer

2.2   Experimental Design

2.2.1   Actuator Design

One purpose of this research is to verify plasma actuator flow control models based on theoretical calculations. The constraints on designing the plasma actuator for the experiment needed to represent the theoretical model as closely as possible. Therefore the experimental actuator is based on the model simulations that modeled an area of 4"x3" with the plasma being generated 1.5" into the length of the board. A modeled version of the printed circuit board to be used as the plasma actuator can be seen in Figure 2.2.

The thickness constraint of the plasma actuator was limited to two factors: the ability to have enough dielectric insulating material to prevent arcing between the two electrodes as well as being light and strong enough to support being used as a structure in experimental testing. The thickness constraint was also limited to the amount of layers any particular vendor could print while working within a reasonable budget limit and lead time production. Regardless of layer thickness, the addition of layers in the circuit board resulted in increased price and manufacturing time. As a result, the final actuator design was a two layer circuit board with a thickness of 0.062" composed of a glass reinforced epoxy (FR4) with electrodes in 0.25" widths and 0.001" thickness. The electrodes were produced with a total amount of
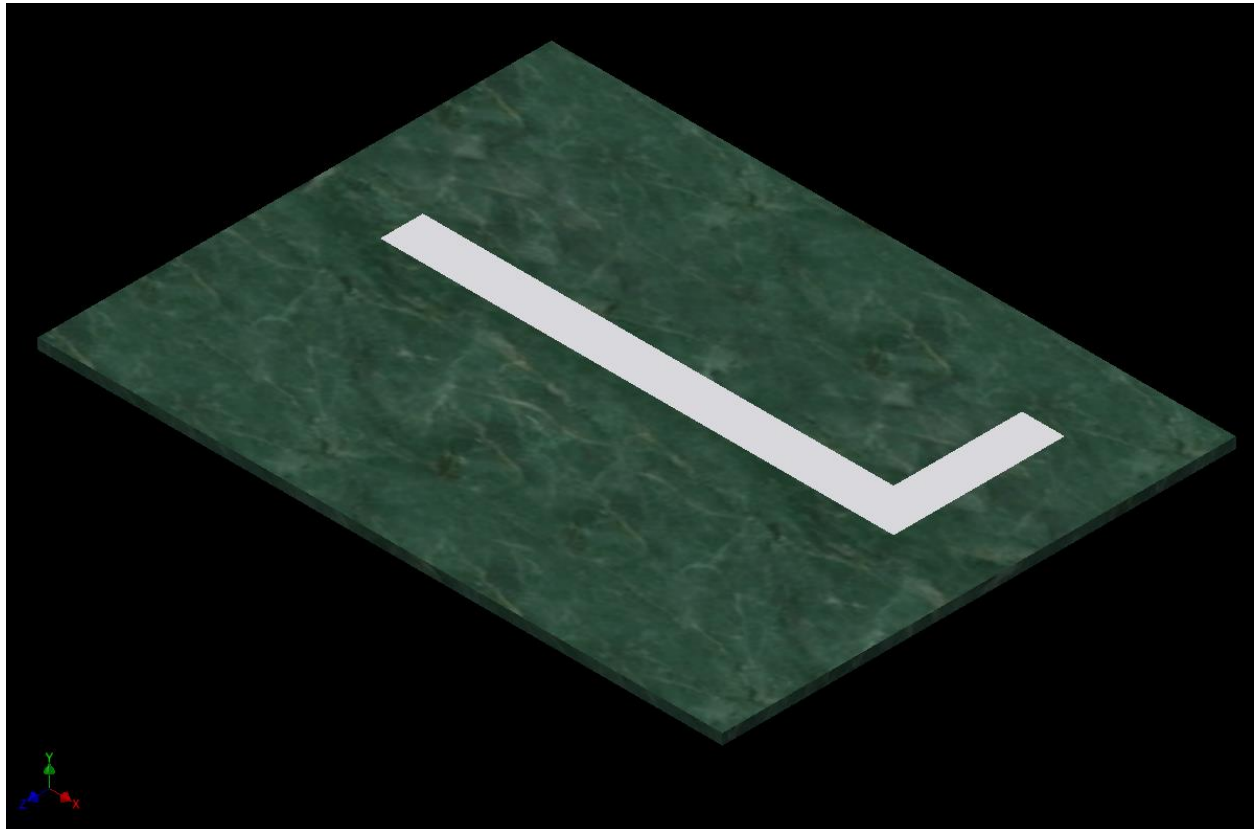
Figure 2.2: An isometric view of Inventor model of the plasma actuator board with dimensions of four inches in the x direction, three inches in the z direction, and 0.062 inches in the y direction.

1 oz. of copper material as the conducting element. The Figure 2.3 shows the final plasma actuator board.

Figure 2.3: The final actuator design consisting of two layers of FR4 material encompassing two electrodes. Picture shows the top side of the actuator with the exposed electrode where the plasma will be generated.

2.2.2   Quiescent Design

Since experiments for verifying the flow control simulations required conditions where flow over a range of air velocities was required, it was also necessary to test the actuator in a quiescent environment that represented the model constraints of no moving air. For designing the quiescent actuator setup, two designs were produced. The first design was a complete enclosure around the actuator using optically clear cast acrylic material and the actuator board was used as the base plate. The inside of the enclosure would be completely sealed from the air outside using heavy duty epoxy resin so as to ensure quiescent conditions. The final assembled quiescent enclosure with acrylic is shown in Figure 2.4. The primary constraint for using optically clear cast acrylic material was so that flow conditions within the box could be observed using shadowgraphy. Additionally, it was found that it was necessary to specifically use a cast material as opposed to a extruded material due the lattice structure composition being less deformed in the casting process. The casting process refracted light to a much less degree than a extruded material. However, one drawback to cast acrylic was that it absorbed light in the lower near ultra-violet light spectrum, which is where the majority of the spectrum of the plasma is produced for this plasma actuator setup. [20, 45]

Due to the limited light transmission near the ultra-violet light spectrum, it was necessary to design and build a secondary quiescent setup for the purpose of using spectrometry to take data. Constraints for designing the second quiescent setup were to securely hold and stabilize both the fiber-optic cable from the spectrometer while also holding the actuator during testing. A simple open enclosure that limited the plasma actuator in all of the
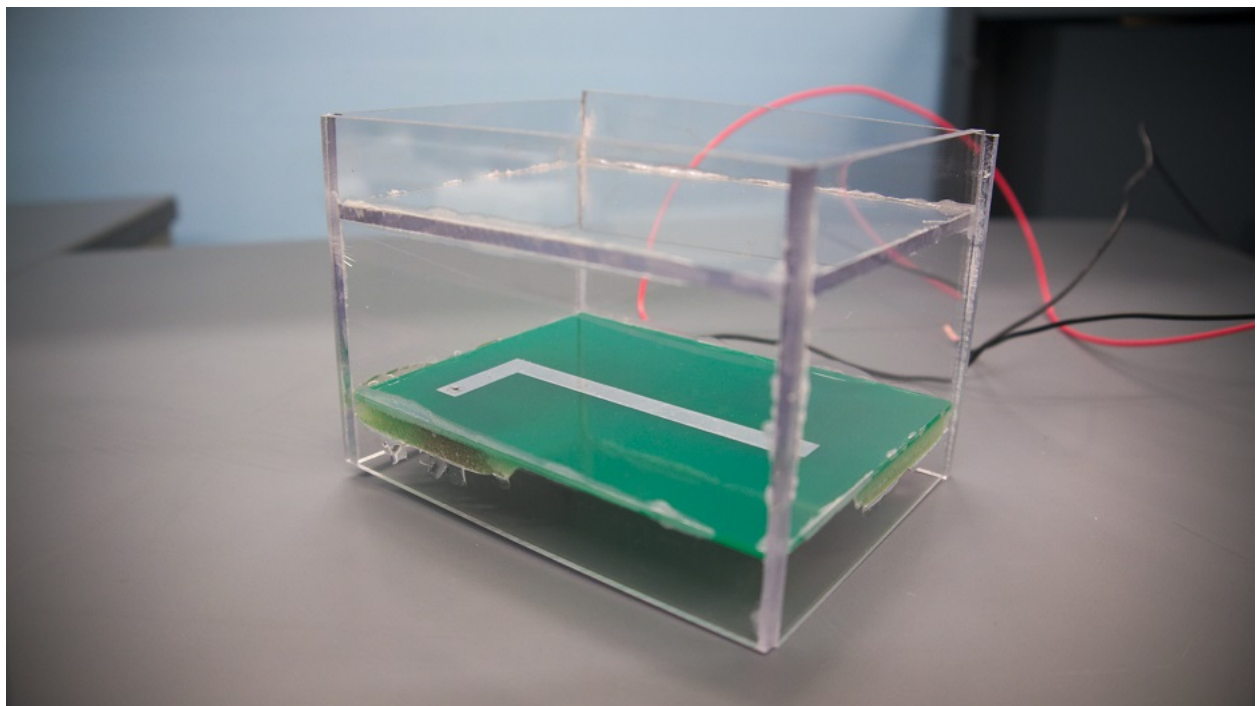
Figure 2.4: Picture of the sealed acrylic enclosure with the actuator for use in shadowgraphy measurements.

degrees of freedom minus one was designed as seen in Figure 2.5. The open degree of freedom allowed for insertion and alignment of the actuator with the spectrometer. The spectrometer was secured through a compression fitted sleeve that pointed directly down towards the actuator. The sleeve was secured to the open enclosure through extruded arches from the farthest four corners from the center as to ensure the flow is not obstructed. The final design was 3D printed in ABS plastic using Stratasys Dimension uPrint 3D Printers available on the Virginia Tech campus.
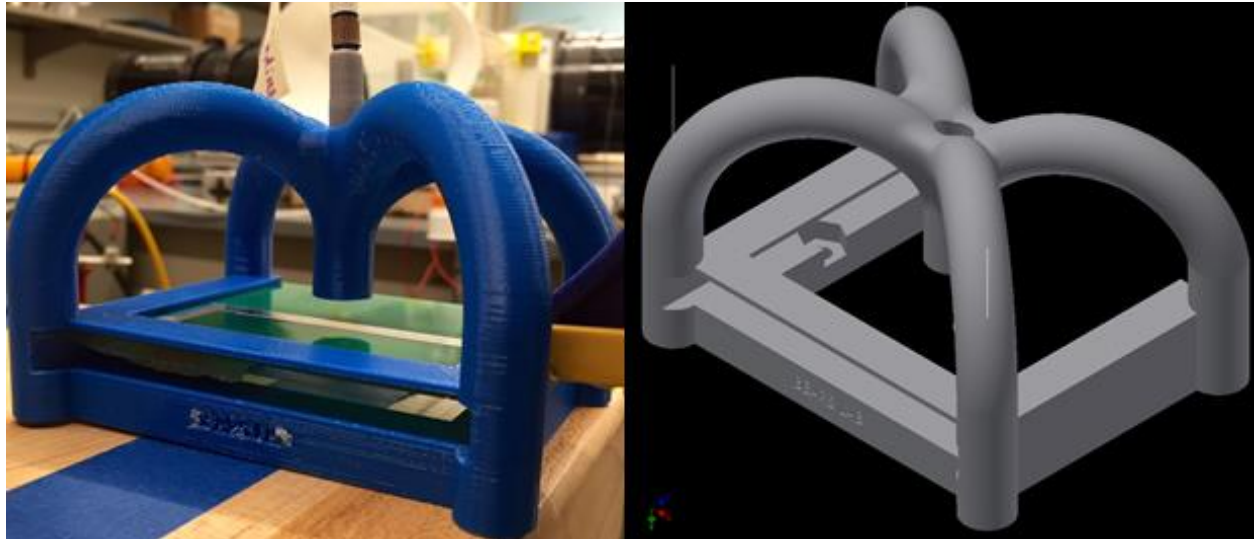
Figure 2.5: On the left, the final quiescent design with the actuator and fiber-optic sensor installed. On the right, shows the actuator holder in the design stage in Autodesk Inventor

To ensure the setup was in a quiescent space while testing, a hand built dark chamber was used as shown in Figure 2.6. The dark chamber consisted of sheathing insulation that had been coated with a matte black paint to help reduce light pollution that might affect
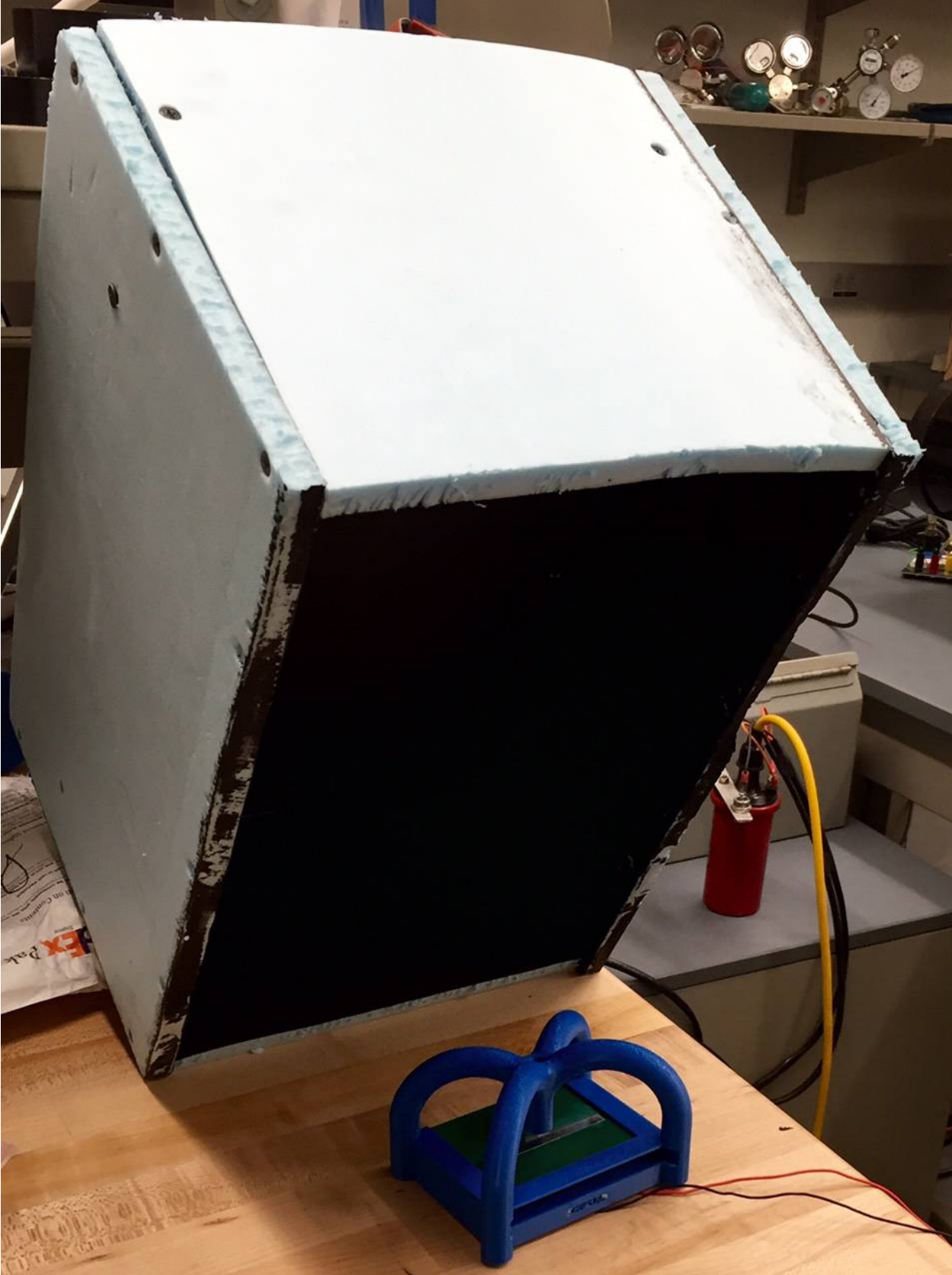
Figure 2.6: The dark chamber built to encompass the quiescent actuator setup.

the spectrometer experiments. In addition to the enclosure to the dark chamber, pressure sensitive tape was used around the seams to ensure quiescent conditions within the chamber.

2.2.3 Flow Design

The flow tunnel was designed with the purpose of testing the actuator at a variety of flow speeds while trying to maintain a laminar wall boundary conditions. It was important to design the flow tunnel to maintain laminar wall boundaries since the theoretical plasma actuator model is simulated under laminar wall boundary conditions. The test section that housed the actuator was designed similar to the quiescent setup using the cast acrylic material minus the walls before and after the actuator to allow for air travel across the actuator as seen in Figure 2.7. Acrylic was used again to ensure that light in the shadowgraphy testing was accurate and clear. In addition, the top and bottom were mounted with acrylic tabs for securing to the honeycomb section. To ensure the test section was under laminar wall boundary layer conditions, the Reynolds number was calculated using equation 2.1 for a variety of speeds that the actuator will experience based on the velocity of air.

$$Re_x = \frac{Ux}{\nu} \tag{2.1}$$

Where the Re_x is the Reynolds number for laminar wall boundary conditions, U is the velocity of the air in the test section, x is the distance away from the actuator strip where the plasma is being generated, and ν is the kinematic viscosity of air. [16] Using pressures

Table 2.1: Total range of velocities based on the total percent of output from the shop vacuum,

and respective Reynolds number generated

Vaccuum (% of Max Power)	Pressure $(h2o)$	Pressure (Pa)	Velocity (m/s)	Reynold's #
80 %	0.090 $in.of(h2o)$	22.42 (Pa)	6.10(m/s)	15397
70 %	0.073 $in.of(h2o)$	18.26 (Pa)	5.51(m/s)	13895
60 %	0.058 $in.of(h2o)$	14.50 (Pa)	4.91(m/s)	12381
50 %	0.045 $in.of(h2o)$	11.21 (Pa)	4.31(m/s)	10887
40 %	0.035 $in.of(h2o)$	8.72 (Pa)	3.81(m/s)	9602
30 %	0.020 $in.of(h2o)$	4.98 (Pa)	2.88(m/s)	7258
20 %	0.011 $in.of(h2o)$	2.74 (Pa)	2.13(m/s)	5383
10 %	0.005 $in.of(h2o)$	1.25 (Pa)	1.44(m/s)	3629

taken with a Dwyer Model 400 manometer at a range of velocities produced from the induced flow from the shop vacuum, the Reynolds numbers were calculated to be well below the transition to turbulent wall boundary range of $2x10^5$ to $3x10^6$. A total list of measured velocities and Reynolds numbers can be seen in Table 2.1, where the maximum output from the 3.5 horsepower shop vacuum was able to generate a pressure of 22.42 pascals in the flow tunnel setup, equaling to a Reynolds number of 15,397. In order to determine the distance away the actuator needed to be away from the walls of the structure to avoid interfering with the boundary layer thickness, equation 2.2 was used.

$$\frac{\delta}{x} = \frac{5.0}{\sqrt{Re_x}} \tag{2.2}$$

Where δ is the the boundary layer thickness, x is the distance along the streamline path of the actuator plate, and Re_x is the Reynold's number for the wall boundary. For laminar wall

conditions under a minimum expected air velocity speed of 1 meter per second, the largest

expected boundary layer thickness is approximately 0.35". So to ensure the boundary wall

layer does not affect the plasma generated, the walls were designed to be one inches away.
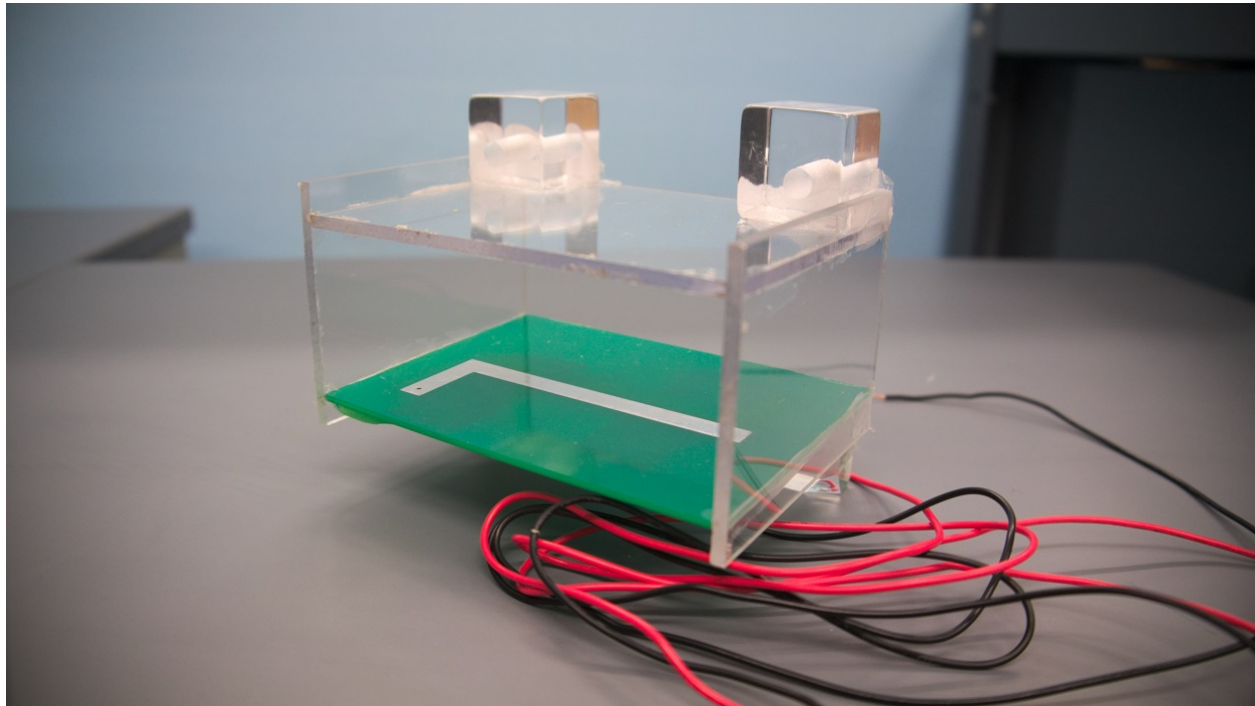
Figure 2.7: Test section for the actuator for use in the flow tunnel.

The piece that held the test section with the actuator consisted of a 3D printed rectangular

section that was 6"x5" in width and length. The width and length were chosen to be at least

25 percent greater than the test section size to ensure air circulating past the test section

would not be affected by turbulence and blockage. [21] In addition, the honeycomb section

had a depth of 2.5" which was filled with partitions throughout the piece that resembled that

of a honeycomb from a bee hive. Each honeycomb was designed with a hydraulic diameter

using equation 2.3 to be a quarter inch in diameter.

$$D_H = \frac{4A}{P} \tag{2.3}$$

Where A is the the cross sectional area, and P is the wetted perimeter based on a quarter inch diameter tube. The purpose of the honeycomb section, as seen in Figure 2.8 is to stabilize turbulent air generated by the shop vacuum, which was connected using a large 3D printed rectangular to circle adapter. The honeycomb section acts as an air straightener so to ensure laminar airflow upstream of the vacuum.
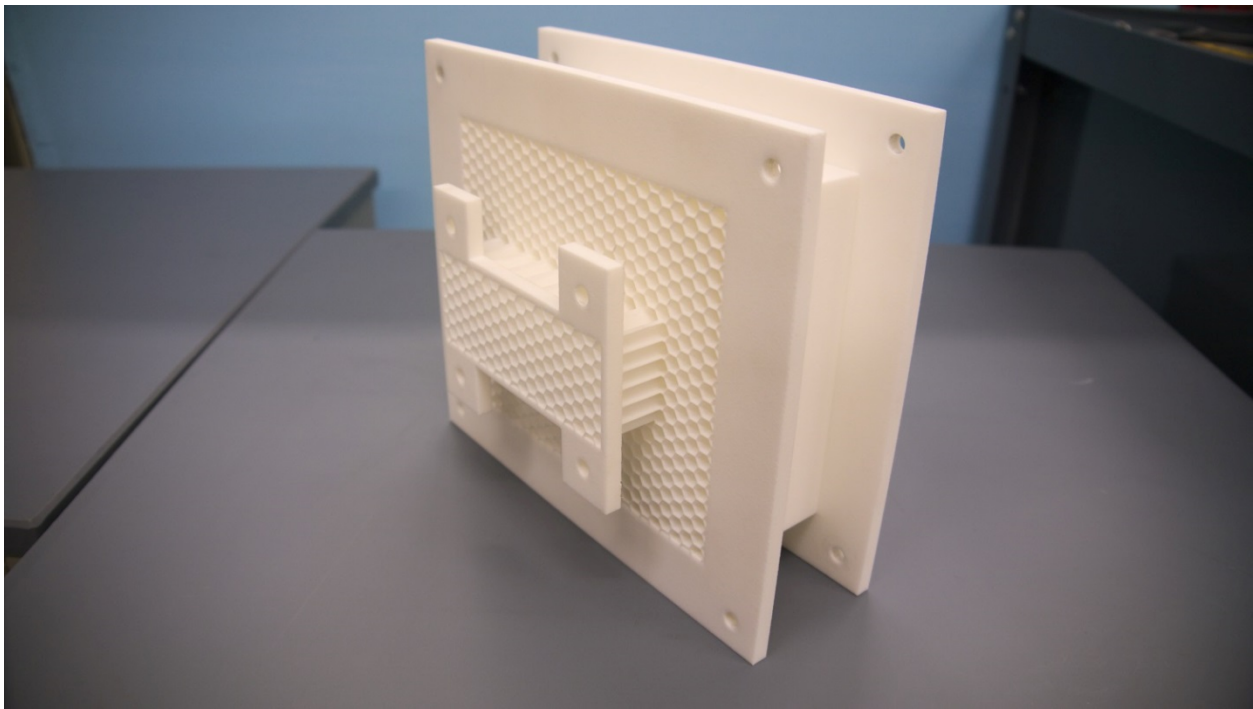
Figure 2.8: Picture of the final honeycomb section that was printed from powdered nylon. Mounting points from the extended honeycomb section can be seen for mounting the test actuator.

In order to properly mount the test section to the honeycomb section, the honeycomb was extruded out away from the body of the piece along with four tabs for securely suspending the test section away from any potential wall turbulence effects. [22]

In addition to the honeycomb section, the test section was also enclosed by a 12" long clear acrylic chamber that helped join the honeycomb section to the bell mouth inlet. The bell mouth inlet helped ensure laminar wall boundary conditions by further reducing turbulent air generated by leading edge effects. The bell mouth inlet was designed according to ASME long nozzle sizing dimensions seen in Figure 2.9. [23]

Since all of the flow tunnel pieces such as the honeycomb, inlet nozzle, and adapter to the shop vacuum were unique to this experiment, they were made using additive manufacturing with powdered nylon. The additive manufacturing of these parts was chosen to due to the complexity and uniqueness of the design of the parts such as the honeycomb piece. Additionally, 3D printing of the parts ensured the parts would be durable and accurate to the intended design specifications.

2.3   Data Collection and Processing

Once the plasma actuators were assembled, data collection for spectral data involved: activating the actuator, recording the outputted voltage and current, and activating the spectrometer software to record the spectral data from the plasma generated. Once the spectral

Inlet Bellmouth
(ASME Long Nozzle)

r_2

c_L

r_1

L_t

d

$r_1 = d$

$r_2 = \frac{2}{3}d$

$L_t = 0.6d$
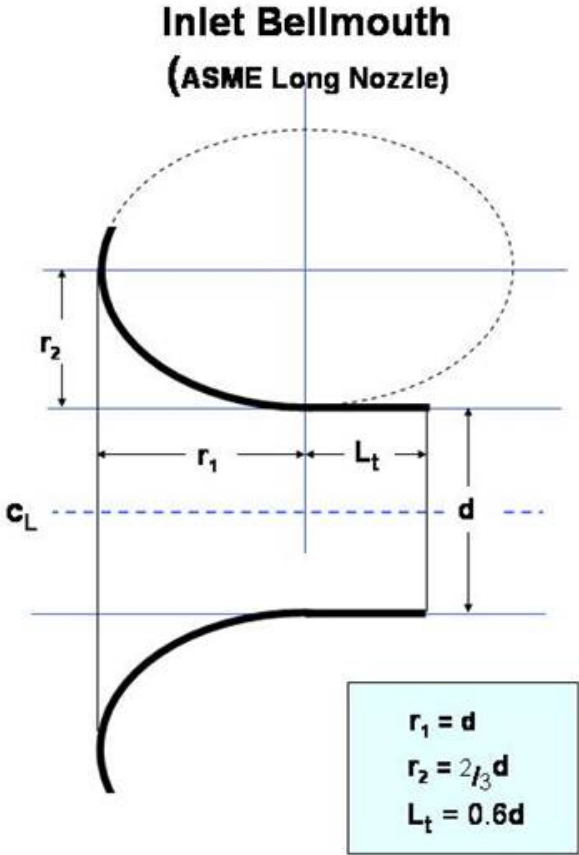
Figure 2.9: ASME bellmouth inlet design for long nozzle setup. Image from ASME Standards

Measurement of Gas Flow by Bellmouth Inlet Flowmeters [23].

data was collected using the spectrometer, the data could then be imported into Excel to be organized by wavelength versus intensity. Once the data was transferred into Excel and organized, the data could then be imported into the Mikropack Specline software for processing and for determining spectral peaks and their associated elements. Using the Mikropack Spekline software, a raw unidentified spectrum can be generated as seen in Figure 2.10. Figure 2.11 shows a sample output of spectral data within the wavelength range of $300nm$ to $450nm$ versus intensities of arbitrary units with known N2 Positive from the Specline database identified. [28, 38-44]
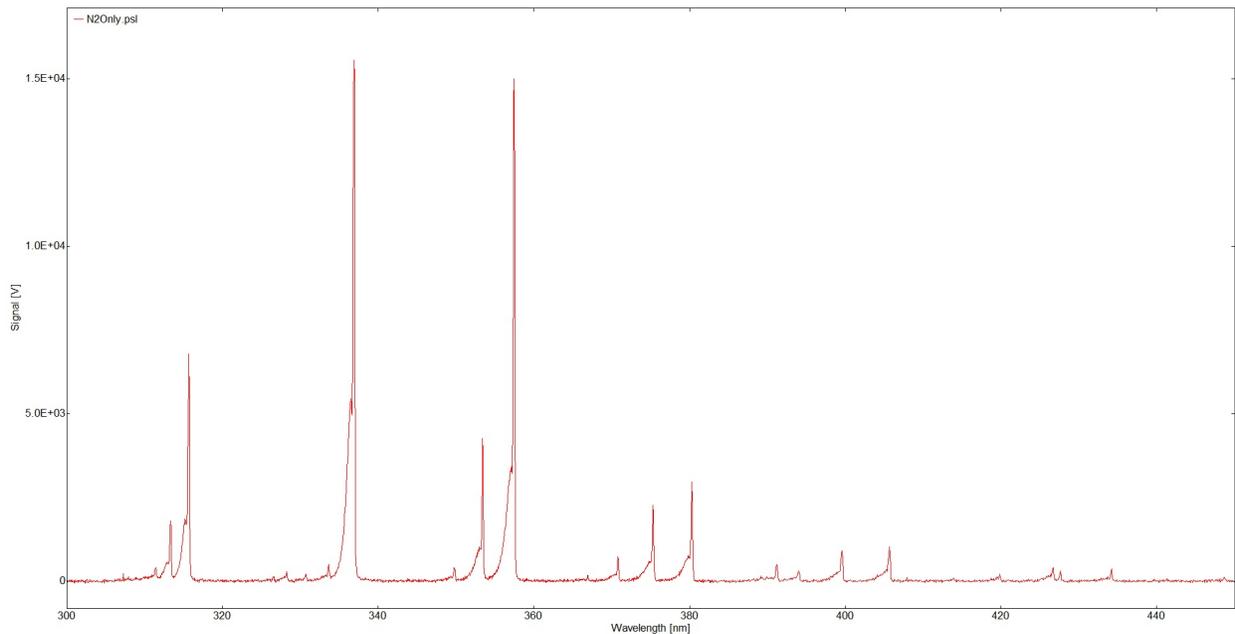
Figure 2.10: A sample outputted spectral peak plot provided by the Mikropack Specline software with raw unidentified intensity peaks of arbitrary units in the y-axis within the range of 300-450 nm in the x-axis.
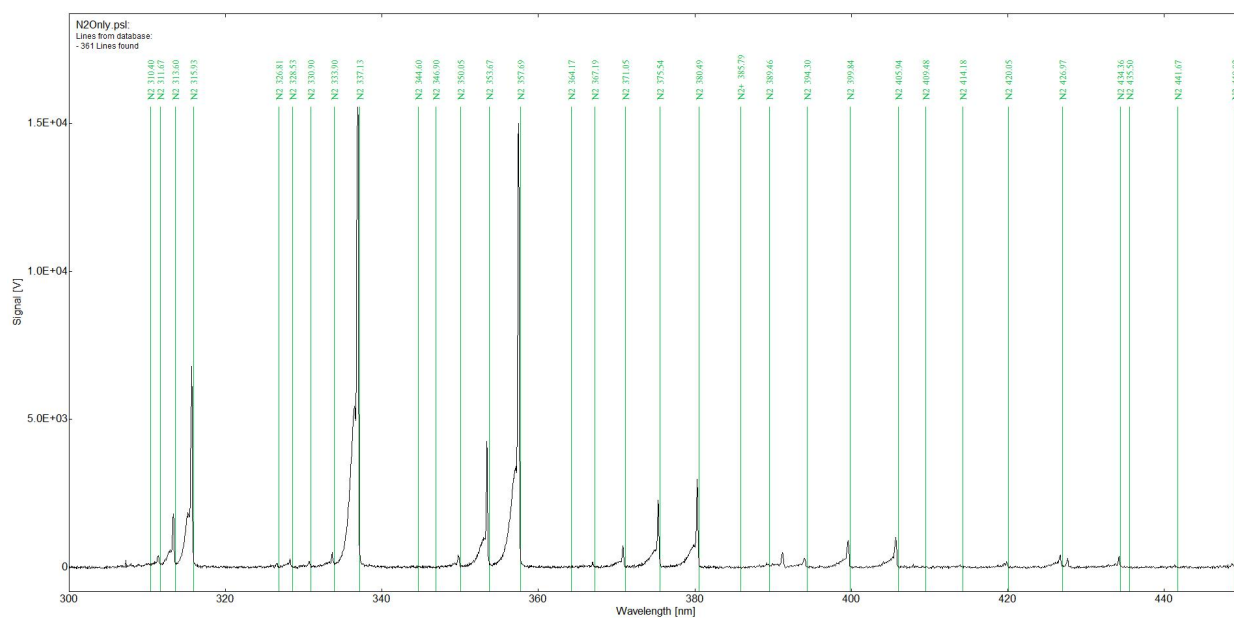
Figure 2.11: A sample outputted spectral peak plot provided by the Mikropack Specline software with the known N2 positive peaks identified intensity peaks of arbitrary units in the y-axis within the range of 300-450 nm in the x-axis.

2.4   Plasma Parameters

2.4.1   Electron Temperature

The electron temperature in plasma can be quantified using the relative line intensity ratio method, which uses the intensities two of atomic lines taken from spectral data. The lines being used should be of the same element and far enough apart in the spectrum to not affect each other through broadening effects. Using a ratio of the line intensities with the assumption of local thermodynamic equilibrium, and a Boltzmann distribution of intereactions at upper energy levels leads to equation 2.4;

$$kT_e = \frac{(E_1 - E_2)}{ln(\frac{I_2 g_1 f_1 \lambda_1^3}{I_1 g_2 f_2 \lambda_1^3})} \tag{2.4}$$

where kT_e is the electron temperature in (eV), the E_1 and E_2 are the upper level energies of the respective lines in the spectrum being measured in (eV), I_1 and I_2 are the relative intensities of the lines, λ_1 and λ_2 are the wavelengths of the emitted lines in (nm), g_1 and g_2 are the statistical weights of the respective lines, and f_1 and f_2 are the oscillator strengths. The relationship between the statistical weights and oscillator strengths, gf, can be determined from the transition probability relationship in equation 2.5,

$$g_i f_i = 1.499x10^{-8} A_i \lambda^2 (2J+1) = 303.8\lambda^{-1}S \tag{2.5}$$

where i refers to the upper level energy levels of the emitted lines, Ai is the transition probability in s^{-1}, λ is the wavelength of the respective line, J is the quantum number of the emitted line, and S is the line strength. [24, 37, 40]

2.4.2   Electron Density

In order to quantify the density of the atmospheric plasma with spectroscopic data, two methods will be discussed; the Stark Broadening and Vibrational method, both of which can be used to calculate the electron density under conditions specific to each method. The first method to calculate the electron density is through the use of the Stark Broadening method. The Stark broadening method, sometimes known as the pressure broadening method, is a more common and less mathematically intensive way to determine the electron density through the use of extensive tables provided by Griem's *Plasma Spectroscopy.* Typically when analyzing spectra that are from hydrogen lines such as the H-α, H-β, and H-γ the electron density can be determined using the linear Stark effect relationship in equation 2.6,

$$N_e = C(N_e, T_e)\Delta\lambda_{FWHM}^{3/2} \tag{2.6}$$

where, N_e is the electron density, C is a constant parameter that weakly depends on electron temperature and density, and $\Delta\lambda_{FWHM}$ is the full width half maximum of the line being inspected. The constant C can be found in reference tables from Griem's *Plasma Spectroscopy.* Normally through the use of the H-β line, the density of electrons can be calculated with an error of approximately 5% - 10%. When looking at spectra from non-hydrogen like atoms, a linear relationship can no longer be used to determine the electron density, and the Quadratic Stark Effect relationship between the electron density and the width of a line must be used, which is given by,

$$\Delta\lambda_{FWHM} \approx 2\left[2 + \frac{1.75 * n_e^{\frac{1}{4}}\alpha}{10^4}\left(1 - \frac{0.068 * n_e^{\frac{1}{6}}}{T^{1/2}}\right)\right] * \frac{w * n_e}{10^{16}} \tag{2.7}$$

where $\Delta\lambda_{FWHM}$ is the full width half maximum of the line being inspected, n_e is the electron density, α is the ion broadening parameter, T is the temperature in Kelvin, and w is the electron-impact half width parameter. The first term within the brackets in equation 2.7 is the electron interaction in the plasma. The second term within the brackets is the contribution from ion broadening, which is normally small and negligible. Thus when neglecting effects from ion broadening equation 2.7 can be simplified to:

$$\Delta\lambda_{FWHM} \approx 2 * 10^{-16} w n_e \tag{2.8}$$

The parameters α and w are found from the tables of Stark-broadening parameters for isolated visible lines of neutral and singly ionized atoms in Griems *Plasma Spectroscopy*. [37, 40]

The second method in determining electron densities from a plasma is through the use of the vibrational method. If the spectra generated from the plasma has primary contributions from the vibrational transition states of an atomic or diatomic species, such as Nitrogen, then these transition states will receive and give off photons in a similar way photons are emitted from excited atoms through collisions. If vibrational transition states are a primary contributor to the analyzed spectrum, then distinct peaks from transitional bands can be used to identify the type the spectrum such as in Figure 2.11 mentioned previously.

If the primary constituents from the vibrational method are known, then equations 2.9 and 2.10 can be used to determine the electron densities.

$$\int_{bandwidth} I_\lambda d\lambda = n_{N_2} n_e k_{exc} \frac{A_{N_2(C-B,0-0)}}{A_{N_2(C-B,0)} + k_{N_2}^{O_2} n_{O_2}} \tag{2.9}$$

$$k_{exc} = 4 * \pi * \sqrt{2} \int_E f_v(E, T_e) \sqrt{\frac{2q}{m_e}} E \sigma_{exc}(E) dE \qquad (2.10)$$

where I_λ is the intensity of the vibrational transitional band taken over the respective band-width range of the species, n_{N_2} is the number density of the N_2 molecules, n_e is the electron density, k_{exc} is the probability rate of excitation of the molecule based on collision cross-sections, A is the atomic transition probability of the respective molecules and atoms which can be found in tables, $f_v(E, T_e)$ is the distribution of electron energies, which for low electron temperatures are assumed to be Maxwellian, σ_{exc} is the excitation cross-section at some energy, q is the electron charge, and m_e is the mass of the electron. [47-49]

Chapter 3

Optical Emission Spectropy of Atomspheric Plasmas Create Via Pulsed-DC Actuators

This section contains a paper to be submitted to IEEE Plasma Science

3.1   Equipment Specifications

Abstract

The concept of plasma flow control is a relatively new idea based on using atmospheric plasma placed near the edge of an air foil to reduce boundary layer losses. Currently there

are a variety of experiments being done to better understand plasma flow control. Of primary importance is to measure the plasma electron temperature and number density of the plasmas generated by these actuators. The primary focus of this work is to design, build and test plasma actuators in order to determine the plasma characteristics relating to electron temperatures and densities using optical emission spectroscopy.

3.2 Introduction

Optical emission spectroscopy (OES) is an *in situ*, non-invasive diagnostic technique that uses atomic emissions to determine the elemental composition of a sample. In this paper, the sample being studied is atmospheric plasma produced using a pulsed Direct Current (DC) Dielectric Barrier Discharge (DBD) actuator. The atmospheric plasma created using a DBD actuator has a wide variety of applications in flow control within gas turbines, struts, airfoils, inlets, and a variety of low Reynolds number flow applications [1]. Although the research in this paper is with flow control using a DBD actuator in mind, atmospheric plasmas have additional interests that include, but are not limited to, the bio-medical and environmental industry for controlling air pollution, waste water cleaning, bio-decontamination, material/surface treatment, electromagnetic wave shielding, and nanotube growth [2]. Since the current use of DBD actuators as a form of plasma generation for flow control is still a relatively novel technique, this study will focus on the ability to quantify the generated plasma using OES to allow for the validation and comparison of important plasma parameters in

on-going and concurrent research of multi-physics modeling of DBD flow control actuators. This is of particular interest as these measurements are generally difficult to achieve without the use of argon or other seed gasses to determine temperature and density under similar conditions.

3.3   Experimental Setup

The optical emission equipment consists of a Ocean Optics LIBS2500Plus Spectrometer, which has a spectral range of $200-980nm$, with a resolution of approximately $0.1nm$(FWHM) and a sensitivity of parts-per-billion and picogram levels. OceanView software is used to manage and record the data outputted by the LIBS2500Plus Spectrometer, and Mikropack Specline is used to analyze the raw spectral data to determine the individual constituents in the generated plasma. To gather data, a B&K Precision 4030 10Mhz Pulse Generator, Tektronix TPS2024B Oscilloscope, Dell 135w PSU, Tektronix P6015A High Voltage Probe were used. The plasma actuator setup consists of a custom printed seven layer printed circuit board. To hold, stabilize and align the spectrometer sensor with the actuator, a cradle for the actuator and spectrometer fiber optic cable was designed and printed in ABS plastic using additive manufacturing from a Stratasys Dimension uPrint 3D Printer.

3.3.1 Plasma Actuator

The dielectric barrier discharge actuator used for this work is depicted schematically in Figure 3.1. This actuator design was fabricated using a printed circuit board (PCB) with an FR4 (glass-reinforced epoxy) dielectric. As power is sent via a pulsed DC voltage source through the red electrode within the circuit board and grounded via the black electrode, the exposed side of the black electrode ionizes the air within its vicinity to generate an atmospheric plasma that moves from left to right in this case.
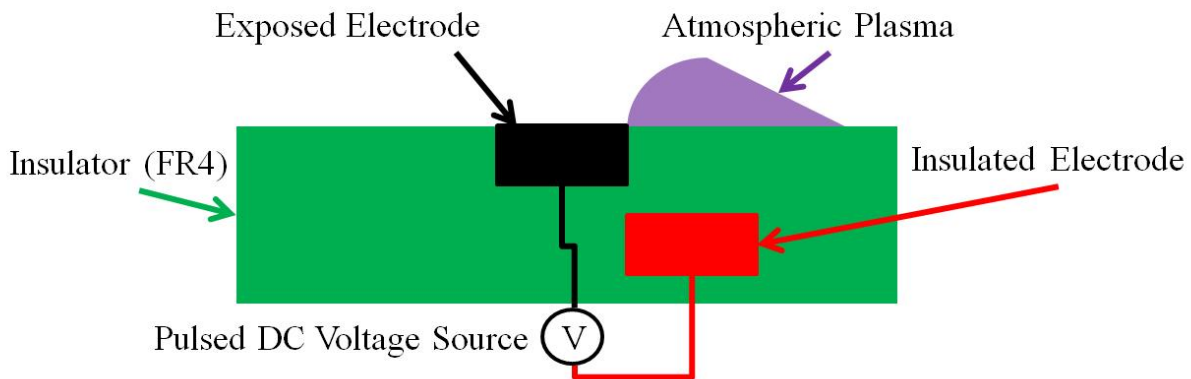
Figure 3.1: Schematic of a basic DBD plasma actuator where the insulator is a typical FR4 circuit board layer that acts as the dielectric barrier encompassing the ground and input electrode.

To keep the electrical connections away from the flow control region, the electrode connection points were located on the bottom, with internal connections routed to keep the connection points away from the plasma region. A photograph of the actuator is shown in Figure 3.2. The plasma actuator was also designed to eventually be used in flow experiments and for

validation of a computational code. The flow passage experiment was designed to observe the effects of the DBD actuator in the presence of flow over its surface, so the dimensions were chosen such that the test article would have equivalent dimensions to the eventual simulation environment. The channel was designed to have the same cross sectional dimensions (3" streamwise direction by 1.5" normal direction) as the computational model, and to have a longer spanwise dimension as a rough approximation to an infinite depth dimension (4").
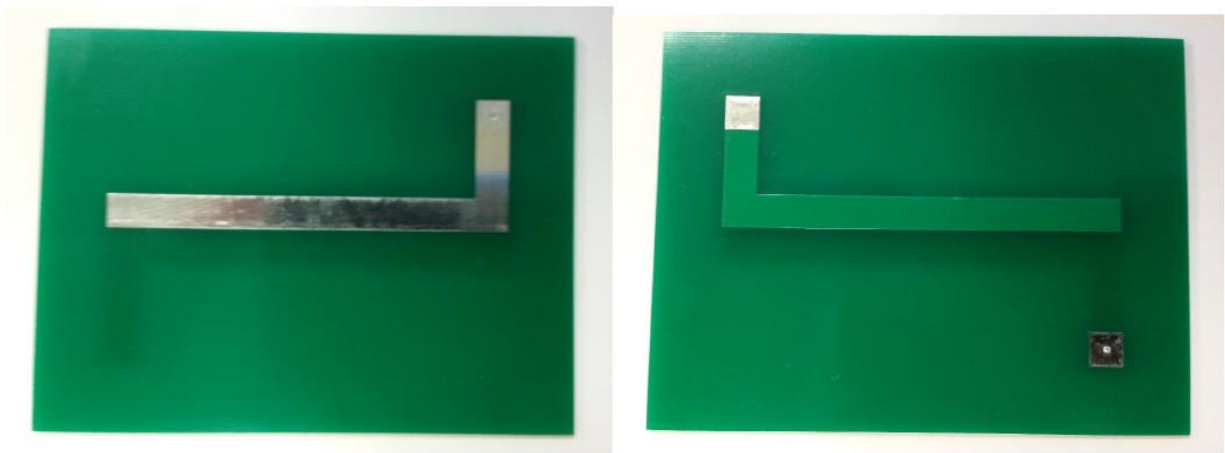
Figure 3.2: Photograph of the printed actuator circuit showing flow side (left) and under side (right).

The power supply for the actuator was built form two automotive capacitive discharge ignition modules. The modules were synchronized using a T-flip flop circuit connected to the desired clock signal generated by a B&K 4030 clock generator. Rectifying diodes were applied prior to the step-up ignition coil and the output of the coil was connected to the actuator. This can be seen in 3.3. The system create negative voltage pulses with an example measured voltage output trace shown in Figure 3.4.
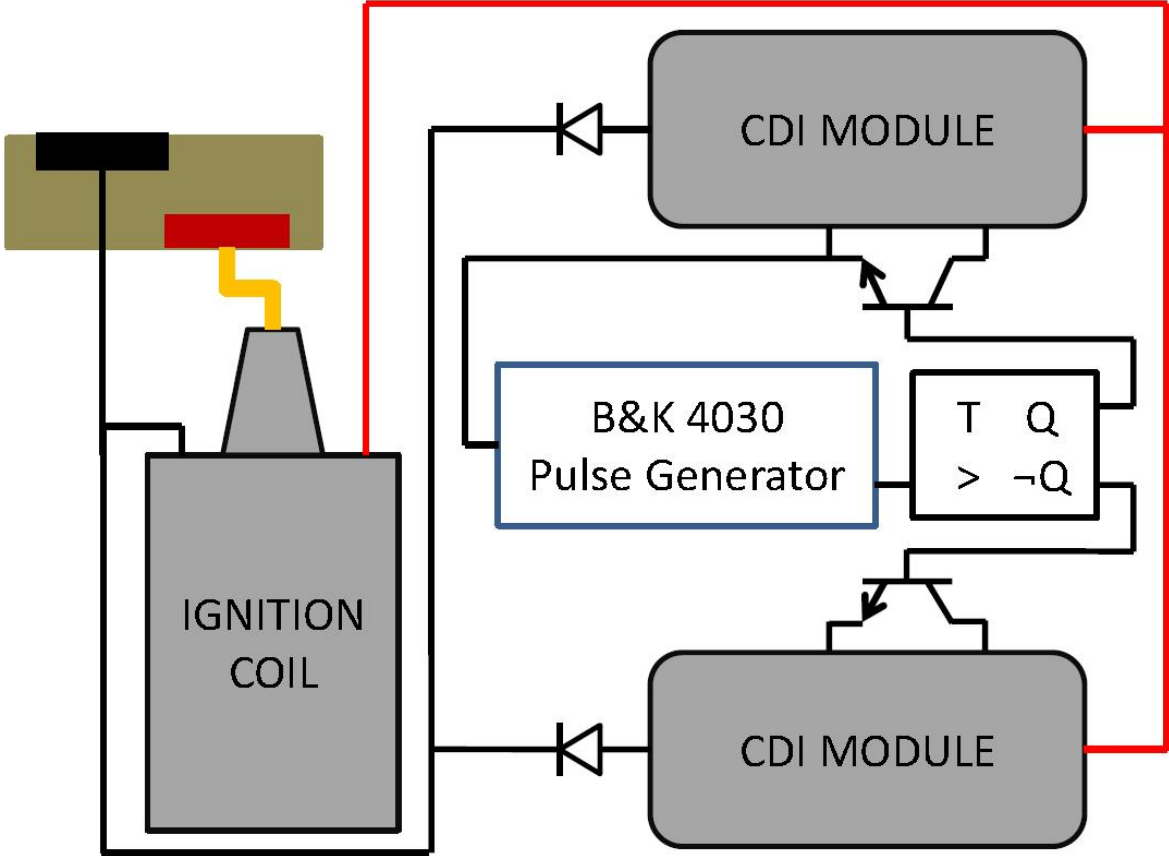
Figure 3.3: Schematic diagram of the power supply used to run the actuator.

Figure 3.4: Sample of measured supply output voltage.

3.3.2 Optical Emission Spectroscopy

In order to measure the emission spectrum of the discharge and better visualize the faint plasma, the tests were conducted and experimental data collected in a darkened laboratory. A high resolution Ocean Optics LIBS2500Plus with 7 HR2000+ modules installed to collect the spectroscopy data. It has a precision of $0.1nm$ and a spectral range of $200 - 980nm$. The dark noise of the system is 12 counts. The window of interest for the spectra collected is between $275nm$ and $425nm$.

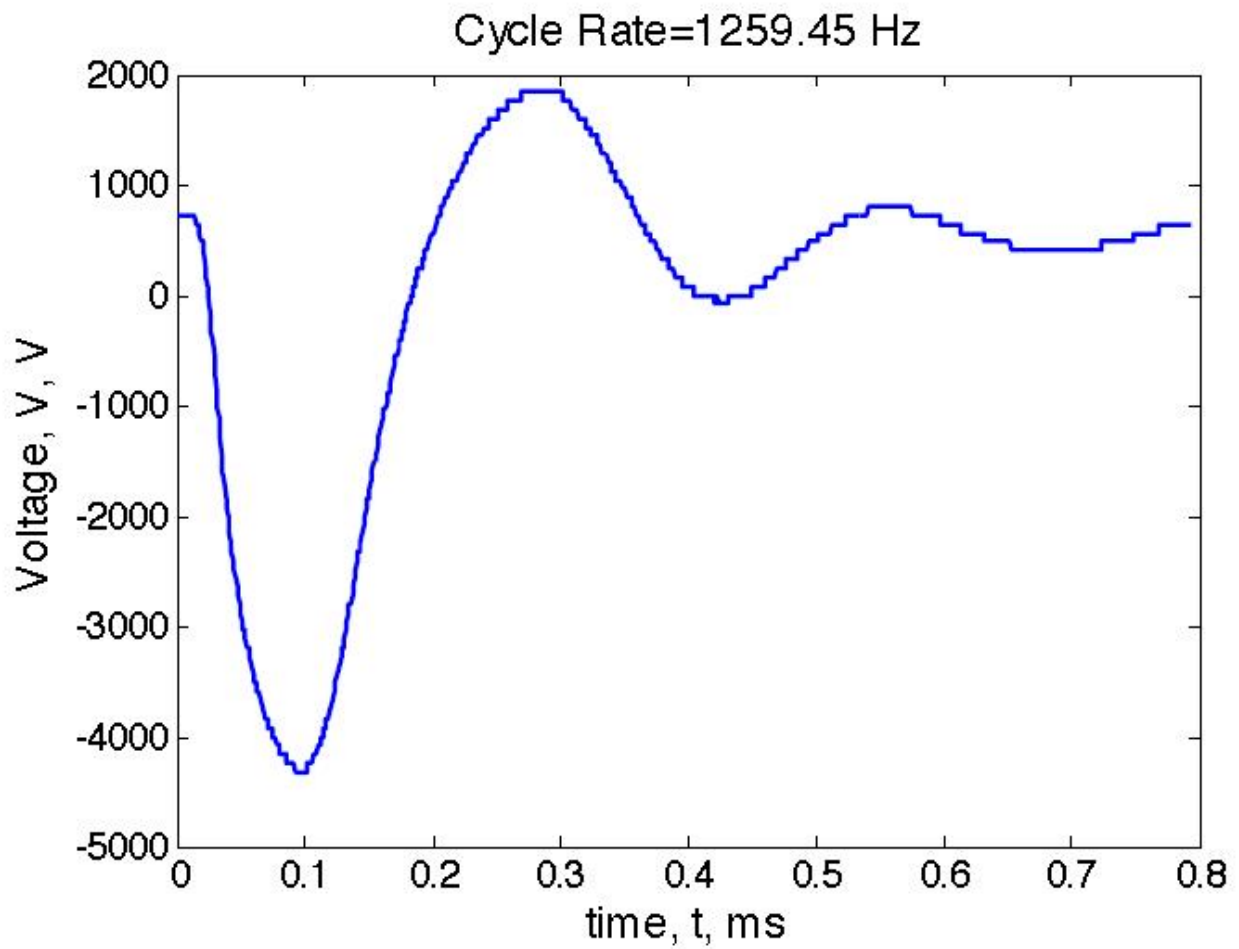Given the relative dim nature of these plasmas, the spectrometer was set to take data over a 10 second period. The peaks of the spectrum were used to compute electron number densities and electron temperature. Due to the minimal hydrogen content of the air, the relative line method and $N_{2(BC;0-0)}$ peak intensity metrics were used to compute the electron number densities and electron temperature. Holding the fiber optic lead steady over the brightest part of the plasma proved difficult, so custom holder was designed and 3D printed to facilitate measurements as shown in Figure 3.5. The actuated plasma during operation can be seen in Figure 3.6.

Additionally, the associated Mikropack SpecLine software package was used to analyze the raw spectral data to determine the constituencies in each peak. The high voltage probe used to measure the actuator applied voltage was a Tektronix P6015A. It was connected to a Tektronix TPS2024B oscilloscope, from which the voltage traces could be saved. An example output from this combination was shown in Figure 3.4.
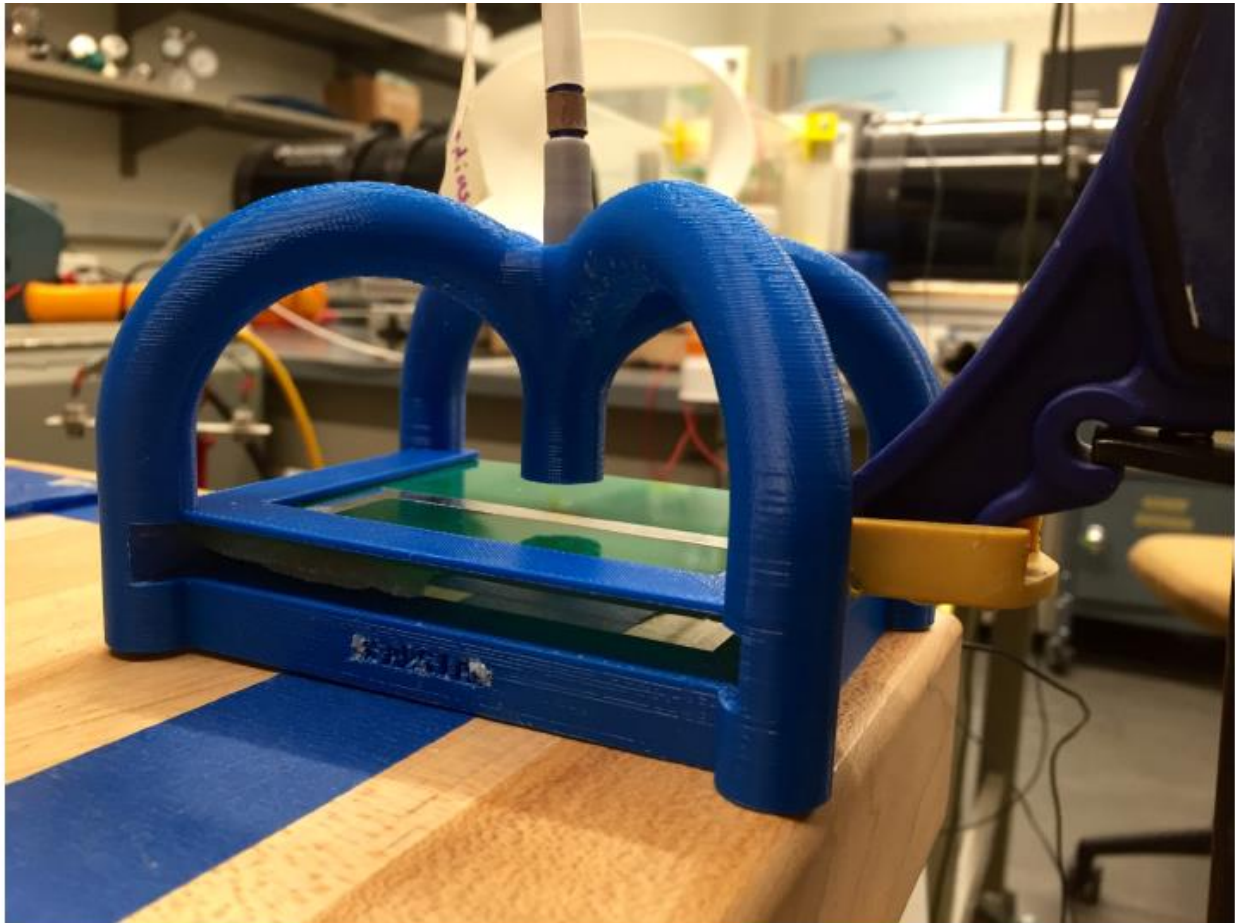
Figure 3.5: Photograph of the spectrometer fiber optic mounted to a test actuator.
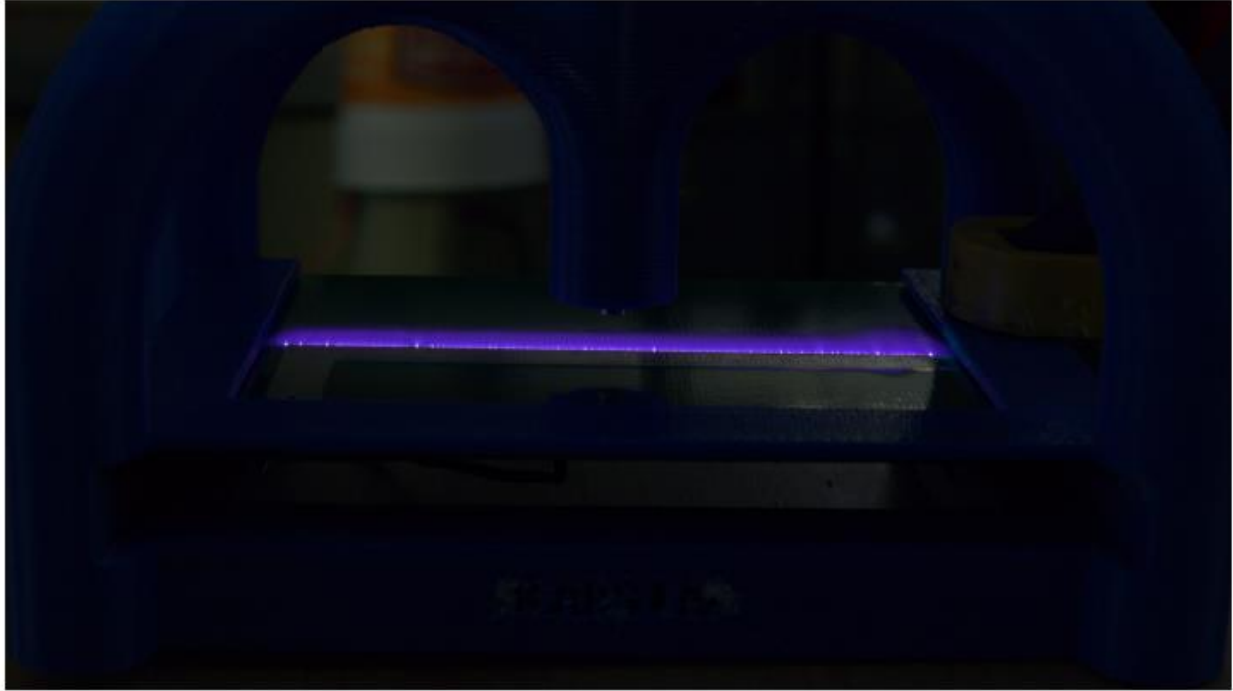
Figure 3.6: Photograph of the spectrometer fiber optic mounted to a test actuator.

3.4 Results

The spectra were processed using the relative line method and an absolute intensity transition method to compute electron temperatures and number densities. An example spectrum can be seen in Figure 3.7. The peaks of the N2 second positive set of transitions are readily identified.

These data were used with the formulation in Eq. 1 to compute the electron temperature. The transitions used to compute the electron temperatures were the $N_{2(BC;0-0)}$ transition at a wavelength of $336.9nm$ and the $N_{2(BC;0-1)}$ transition at a wavelength of $315.7nm$. The intensity values were integrated over a bandwidth of $2nm$ for both peaks. The electron
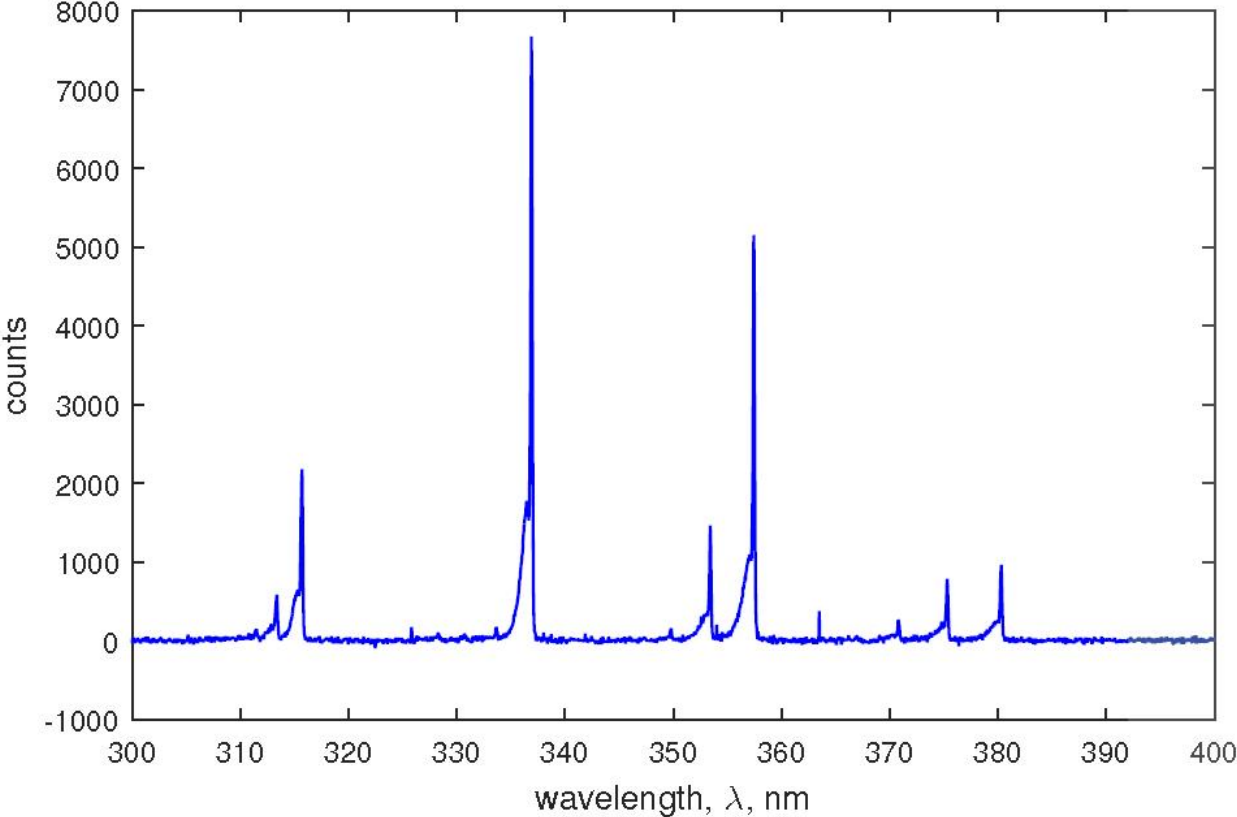
Figure 3.7: Sample emission spectrum.

temperature is calculated using the relative line method [5] using Equation 1. The relative line method utilizes the intensities (I) associated with two spectral lines from the same species along with the energies (E), and the transition probability (A) in s^{-1} of the emitted line.

$$kT_e = \frac{(E_1 - E_2)}{ln(\frac{I_2 g_1 f_1 \lambda_1^3}{I_1 g_2 f_2 \lambda_1^3})} \tag{3.1}$$

The electron number density can be computed from the integrated photon intensity of the $N_{2(BC;0-0)}$ transition in equation 3.2 [6]. The transition probabilities, A, can be found from [1], and the number densities of molecular nitrogen and oxygen are computed using an ideal gas equation of state using mole fractions from the 1976 U.S. Standard Atmosphere [2]. The excitation rate coefficient, $k_{exc}$, can also be found in [6], and is related in Equation 3. The excitation cross section, σ_{exc}, can be found in [4], q and m_e are the electron charge and mass respectively, and $f_v(E; Te)$ is the electron energy distribution function, and for low electron temperatures is approximated to be Maxwellian.

$$\int_{bandwidth} I_\lambda d\lambda = n_{N_2} n_e k_{exc} \frac{A_{N_2(C-B,0-0)}}{A_{N_2(C-B,0)} + k_{N_2}^{O_2} n_{O_2}} \tag{3.2}$$

$$k_{exc} = 4 * \pi * \sqrt{2} \int_E f_v(E, T_e) \sqrt{\frac{2q}{m_e}} E \sigma_{exc}(E) dE \tag{3.3}$$

The first column in the table shows the computed electron temperatures. The average of the electron temperature across all runs computed in this manner is $T_e = 0.252 eV$. Given the variety of possible influences on the quality and intensity of the spectral peaks, a formal determination of uncertainty is generally difficult. However, Greim [3] indicates that for the relative line method an uncertainty of approximately 10% is typical. An estimated percent

error of 2.71% was calculated based on the standard deviation of the 12 tests of the actuator.

Table 3.1: Electron temperatures and number density results, with the mean: $T_e = 0.252eV$ and $ne = 1.07 \times 10^{17} \ [\#/m^3]$

run index	*electron temperature*	*number density*
8	0.257eV	$8.04 \times 10^{16}[\#/m^3]$
9	0.242eV	$7.73 \times 10^{16}[\#/m^3]$
10	0.254eV	$7.56 \times 10^{16}[\#/m^3]$
11	0.241eV	$9.02 \times 10^{16}[\#/m^3]$
12	0.250eV	$1.02 \times 10^{17}[\#/m^3]$
13	0.238eV	$1.03 \times 10^{17}[\#/m^3]$
14	0.241eV	$1.00 \times 10^{17}[\#/m^3]$
15	0.267eV	$1.18 \times 10^{17}[\#/m^3]$
16	0.268eV	$1.32 \times 10^{17}[\#/m^3]$
17	0.268eV	$1.57 \times 10^{17}[\#/m^3]$
20	0.237eV	$1.26 \times 10^{17}[\#/m^3]$
21	0.264eV	$1.25 \times 10^{17}[\#/m^3]$
avg	0.252eV	$1.07 \times 10^{17}[\#/m^3]$

The electron number density was estimated from these electron temperatures and the integrated photon intensity of the $N_{2(B-C,0-0)}$ transition peak at a wavelength of $336.9nm$ over a $\pm 2nm$ bandwidth as described. The estimated electron number densities are shown in Table 3.1. The average of electron number density of these runs is $n_e = 1.07 \times 10^{17}[\#/m^3]$. The associated percent error based on the standard deviation of the 12 runs is 12.91%. This is

in agreement with typical air plasma discharges.

3.5 Conclusion

Through the course of this research, a method to measure and characterize dielectric barrier discharge plasmas was developed and used to quantify an experimental setup. The purpose of this research was to design, build and test a set up where spectroscopic measurements of dielectric barrier discharges could be made without the use of seed gasses. Through testing of the plasma actuators with optical measurement techniques like spectrometry, the necessary data is able to be measured and used in calculating plasma parameters such as electron temperature and electron density and values consistent with those expected in the literature are achieved.

Acknolwedgement

References

[1] P. H. Krupenie A. Lofthus. The spectrum of molecular nitrogen. J. Phys. Chem. Ref. Data, 6(1), 1977.

[2] United States Government. U.s. standard atmosphere, 1976. Technical Report NASA-TM-X-74335, National Oceanic and Atmospheric Admin-stration, National Aeronautics and Space Administration, United States Air Force, 1976.

[3] H. R. Griem. Principles of Plasma Spectroscopy. Cambridge University Press, Cambridge, 1997.

[4] M. Hayashi. Recommended values of transport cross sections for elastic collision and total collisition cross section for electrons in atomic and molecular gasses. Technical Report IPPJ-AM-19, Institute of Plasma Physics, Nagoya University, Nagoya, Japan, 1981.

[5] G. V. Marr. Plasma Spectroscopy. Elsevier, Great Yarmouth, 1968.

[6] H. Bahre P. Awakowicz V. Schulz-von der Gathen N. Bibinov, N. Knake. Spectroscopic characterization of an atmospheric pressure u jet plasma source. J. Phys. D: Appl. Phys., 44(345204):12pp, August 2011.

Chapter 4

Conclusions and Future Work

4.1 Conclusion

The purpose of this research was to design, build and test DC DBD actuators under a variety of flow speeds ranging from quiescent to laminar boundary layer conditions. Using optical measurement techniques like OES, it was possible to gather spectra data on the atmospheric plasma for use in calculating plasma parameters such as electron temperature and electron density. The determination of plasma parameters is important in the validation of concurrent research being performed at Virginia Tech to determine if theoretical plasma actuator models operate under accurate assumptions.

In order to find the electron temperature and electron densities of the atmospheric plasma from the DBD actuators, the spectra contribution from the Second Positive N_2 band was

analyzed in the quiescent and flow actuator setups. For the quiescent design based on 12 experimental runs, an average electron temperature was found to be 0.252 ± 0.007 eV with a standard error of 2.71% with a standard deviation of 0.012 eV, and a average electron density was found to be $1.07\text{x}10^{17} \pm 1.38\text{x}10^{16}$ $\frac{\#}{m^3}$ with a standard error of 12.91% based on a standard deviation of $2.50\text{x}10^{16}$ $\frac{\#}{m^3}$. For the flow tunnel setup, the average electron temperature was measured to be 0.251 ± 0.002 eV with a standard error of 0.85 % and an average electron density of $4.63\text{x}10^{16} \pm 5.25\text{x}10^{14}$ $\frac{\#}{m^3}$.

At the time of writing this paper, the theoretical calculations for the multi-physics modeling of the plasma actuators being done concurrently at Virginia Tech were available for comparison. Comparing the measured experimental electron temperatures and densities with theoretical results, the separate data sets seem to agree with a difference of 13% and 18% for the electron temperature and densities respectively. Since the overall experimental designs were built to be a physical representation of the computational model, the final results from this experiment show that the assumptions in theoretical calculations are reasonable valid.

Additionally, the design and alignment of the shadowgraphy setup allowed for the documentation of the atmospheric plasma for use in determining velocities and analyzing flow structures. The determination of velocities and flow structures is related to the computational modeling of the actuator and beyond the scope of this research, but additional information can be found in the PhD dissertation by Schneck. [46]

To conclude, the goal of this research was to design and build a versatile and modular experimental pulsed DC DBD plasma actuator that exactly modeled computational conditions

and boundaries for the purpose of validating computational work being performed at Virginia Tech. The research outlined in this paper provides a method to gather simultaneous fluid-plasma measurements in difficult to measure plasma conditions without introducing invasive probes or addition of a seed gas for determining plasma parameters. The versatility and modularity of the experimental setup will allow comparison of any future work involving any variant of flow scenario to be simulated for validation purposes.

4.2 Future Work

Currently, the experiments for testing the plasma actuator under quiescent and flow setups has setup the basic ground work for testing plasmas generated using a DBD actuator. There are still improvements that can be made in the optical measurement techniques involving the shadowgraphy and spectrometry to improve data collection speed and overall image clarity, respectively. Additionally, creating a closed flow tunnel loop and being able to create a scaled down wind tunnel setup would allow for additional testing in various conditions.

Chapter 5

Bibliography

[1] W. C. Schneck III, (2012, June). "Flow Control Over a Circular Cylinder Using Pulsed DBD Actuators" In Proceedings of ASME Turbo Expo 2012.

[2] J.J. Wang, K. Choi, L. Feng, T. Jukes, R. Whalley. (2013, July). "Recent Developments in DBD Plasma Flow Control" Progress in Aerospace Sciences.

[3] T. Corke and M. Post. (2005, January). "Overview of Plasma Flow Control: Concepts, Optimization, and Applications" 43rd AIAA Aerospace Sciences Meeting and Exhibit.

[4] Z. Machala, M. Janda, K. Hensel, I. Jedlovsky, L. Lestinska, V. Foltin, V. Martisovitis, M. Morvova. (2007, March). "Emission spectroscopy of atmospheric pressure plasmas for bio-medical and environmental applications. Journal of Molecular Spectroscopy." 243 (2007 pp. 194-201.

[5] C.O. Laux, T.G. Spence, C.H. kruger, R.N. Zare, "Plasma Sources Sci. Technol" 12

(2003) 125-138

[6] U. Fantz, "Basics of plasma spectroscopy" Plasma Sources Science and Technology, 15 October 2006, S137-S147.

[7] D.O.E., "Low Temperature Plasma Science: Not only the Fourth State of Matter but All of Them, Report of DOE Office of Fusion Energy Sciences Workshop." September, 2008.

[8] W.K. Lord. "Flow Control Opportunities in gas Turbine Engines" American Institute of Aeronautics and Astronautics. June, 2000.

[9] F.F. Chen, "Introduction to Plasma Physics and Controlled Fusion Volume 1: Plasma Physics," Second edition, Plenum Press, New York. 1984.

[10] P. Diamond et al, "Modern Plasma Physics Volume 1: Physical Kinetics and Turbulent Plasmas," Cambridge University Press, New York. 2010.

[11] A Fridman and L. Kennedy, "Plasma Physics and Engineering," Taylor and Francis Group, New York. 2004.

[12] J. B. Laten and R. P. LeBeau Jr. "Examination of a plasma actuator model applied to dbd actuators for small aircraft applications." In 53rd ASM. AIAA, January 2015. Paper 2015-1732.

[13] Y. Li et al. "Plasma Flow Control," Aeronautics and Astronautics. Air Force Engineering University of China, China. 2011.

[14] M. Hamer. "Design of Optical Measurements for Electrothermal Plasma Discharges."

Masters thesis, Virginia Tech, 2013.

[15] D. Cremers and L. Radziemski, "Handbook of Laser-induced Breakdown Spectroscopy," John Wiley and Sons Inc. 2006

[16] Ocean Optics, "OceanView HR2000+ Installation and Operation Manual, Ocean Optics," A Halma Company. 2013

[17] A. Mazmumdar, "Principles and Techniques of Schlieren Imaging Systems," Columbia University, Department of Computer Science. July 2011

[18] G.S. Settles, "Schlieren and shadowgraph Techniques: Visualizing Phenomena in Transparent Media." Springer, Second Edition, 2006

[19] Ocean Optics, HR2000+ Data Sheet. Ocean Optics, A Halma Group Company. Florida. http://oceanoptics.com//wp-content/uploads/OEM-Data-Sheet-HR2000+.pdf

[20] Arkema, "Optical and Tramission Characteristics," Altuglas International Arkema Group. 2000.

[21] G.V. Parkinson and N. J. Cook. "Blockage Tolerance of a Boundary Layer Wind Tunnel." Journal of Wind Engineering and Industrial Aerodynamics, 41-44, 1992, 873-884.

[22] Munson et al, 2009, "Fundamentals of Fluid Mechanics," Sixth edition, John Wiley and Sons Inc.

[23] ASME, "Measurement of Gas Flow by Bellmouth Inlet Flowmeters", The American Society of Mechanical Engineers. 2011.

[24] A. Mizioleket al, 2006, "Laser-Inducted Breakdown Spectroscopy," University Press, Cambridge.

[25] H. Griem. 1997, "Principles of Plasma Spectroscopy," University of Maryland, College Park. University Press, Cambridge.

[26] W. Lochte-holtgreven. 1968, "Plasma Diagnostics," North-Holland Publishing Company, Amsterdam. John Wiley and Sons, Inc.

[27] H. Griem. 1974, "Spectral Line Broadening By Plasmas," University of Maryland, College Park. Academic Press.

[28] G. Herzberg. 1950, "Molecular Spectra and Molecular Structure: I. Spectra of Diatomic Molecules," National Research Council of Canda, Van Nostrand Reinhold Company.

[29] G. Marr, 1968, "Plasma Spectroscopy," Reader in Physics, Reading, England. Elsevier Publishing Company

[30] M. Kettani, and M. Hoyaux. 1973, "Plasma Engineering," John Wiley and Sons, Inc.

[31] M. Venugopalan. 1971, "Reactions Under Plasma Conditoins Volume 1," Western Illinois University, John Wiley and Sons, Inc.

[32] R. Hippler, H. Kersten, M. Schmidt, K. Schoenbach. 2003, "Low Temperature Plasmas Fundamentals, Technologies, and Techniques Volume 1," Second Edition, John Wiley and Sons, Inc.

[33] R. Hippler, H. Kersten, M. Schmidt, K. Schoenbach. 2003, "Low Temperature Plasmas

Fundamentals, Technologies, and Techniques Volume 2," Second Edition, John Wiley and Sons, Inc.

[34] J. Wesson. 2011, "Tokamaks," Fourth Edition, Oxford University Press.

[35] V. Ochkin. 2009, "Spectroscopy of Low Temperature Plasma," John Wiley and Sons, Inc.

[36] C. Suplee. 2009, "The Plasma Universe," Cambridge University Press.

[37] J. Singh and S. Thakur. 2007, "Laser-Induced Breakdown Spectroscopy," Elsevier

[38] M.A. Bourham, O. Hankins, J. Gilligan, J. Earnhart. "Visible Light Emission Measurements From a Dense Electrothermal Launcher Plasma," IEEE Transactions on Magnetics, Vol. 29 No. 1. 1993

[39] G. Knoll. 2010, "Radiation Detection and Measurement," Fourth Edition, John Wiley and Sons, Inc.

[40] H. Griem, 1964, "Plasma Spectroscopy," University Press, Cambridge.

[41] A. Sherbini, A. Aamer. "Development of a Simple Software Program Used for Evaluatoin of Plasma Electron Density in LIBS Experiments via Spectral Line Shape Analysis," Journal of Signal and Information Processing, 2012, 3, 502-515.

[42] V. Unnikrishan et al, "Measurements of Plasma temperature and electron density in laser-induced copper plasma by time-resolves spectroscopy of neutral atom and ion emissions," Pramana Journal of Physics, Vol 74, No. 6. June, 2010. Pp983-993.

[43] S. Bayram and M Freamat, "Vibrational spectra of N2: An advanced undergraduate laboratory in atomic and molecular spectroscopy," American Association of Physics Teachers, 80 (8), August 2012.

[44] J. Reader, and C. Corliss, "Wavelengths and Transition Probabilities for Atoms and Atomic Ions," US Department of Commerce. December, 1980.

[45] Makrolon, "Optical Properties of Makrolon and Aspec for non-imaging optics," Bayer material Science AG. 2014.

[46] W. C. Schneck III. Multi-Physics Model of a Dielectric Barrier Discharge Flow Control Actuator with Experimental Support. Ph.D Dissertation, Virginia Tech, January 2016.

[47] S. Keller P. Rajaskaran N. Bibinov P. Awakowicz, "Characterization of transient conditions applying nitrogen photoemission and current measurements." J. Phys. D: Appl. Phys., 44(345204):12pp, September 2011.

[48] J. Kim et al, "Electron density and temperature measurement method by using emission spectroscopy in atmospheric pressure nonequilibrium nitrogen plasmas," Physics of Plasmas, 13, September 6, 2006.

[49] H. Bahre P. Awakowicz V. Schulz-von der Gathen N. Bibinov, N. Knake. "Spectroscopic characterization of an atmospheric pressure u jet plasma source." J. Phys. D: Appl. Phys., 44(345204):12pp, August 2011.